

Galactic magnetic fields I. Theoretical model and scaling relations

LUKE CHAMANDY,^{1,2} RION GLENN NAZARETH,¹ AND GAYATHRI SANTHOSH¹

¹*National Institute of Science Education and Research, An OCC of Homi Bhabha National Institute, Bhubaneswar 752050, Odisha, India*

²*Department of Physics and Astronomy, University of Rochester, Rochester NY 14627, USA*

Abstract

Galactic dynamo models have generally relied on input parameters that are very challenging to constrain. We address this problem by developing a model that uses observable quantities as input: the galaxy rotation curve, the surface densities of the gas, stars and star formation rate, and the gas temperature. The model can be used to estimate parameters of the random and mean components of the magnetic field, as well as the gas scale height, root-mean-square velocity and the correlation length and time of the interstellar turbulence, in terms of the observables. We use our model to derive theoretical scaling relations for the quantities of interest, finding reasonable agreement with empirical scaling relations inferred from observation. We assess the dependence of the results on different assumptions about turbulence driving, finding that agreement with observations is improved by explicitly modeling the expansion and energetics of supernova remnants. The model is flexible enough to include alternative prescriptions for the physical processes involved, and we provide links to two open-source PYTHON programs that implement it.

Keywords: dynamo – galaxies: magnetic fields – galaxies: ISM – galaxies: structure – galaxies: statistics – ISM: magnetic fields

1. INTRODUCTION

Spiral galaxies generally host magnetic fields with strengths of order 10 μ G. The general properties of such fields can be explained using turbulent dynamo models, but detailed comparison between theory and observation is still rudimentary (for reviews, see [Ruzmaikin et al. 1988](#); [Beck et al. 1996](#); [Shukurov 2004, 2005](#); [Van Eck et al. 2015](#); [Beck et al. 2019](#); [Shukurov & Subramanian 2021](#)). The situation can be improved using various complementary approaches. One of them is to evaluate observable quantities using simple, preferably analytic models of galactic magnetic fields, since they are readily available, transparent, easy to apply and can be used to explore the parameter space. However, such models tend to depend on poorly known galactic parameters, such as the turbulent correlation time τ and length l . This problem can now be partially circumvented by using a model for the turbulence parameters ([Chamandy & Shukurov 2020](#)) whose inputs can be expressed in terms of observable quantities.

The point of the present work is to write down a closed set of coupled algebraic equations that can be solved to obtain mag-

netic field properties from a handful of galactic observables, to use these equations to derive scaling relations in certain asymptotic limits, and to compare these relations with those suggested by observations.¹ We make no attempt to include cosmological evolution, and thus our model is restricted to low-redshift galaxies (redshift $\ll 1$).

Magnetic fields can play a role in various aspects of galactic astrophysics given that their energy densities are comparable to those of turbulence, cosmic rays and thermal motions. Scaling relations can be particularly useful in modeling such effects. Take, for instance, the empirical scaling relation between the total magnetic field strength B and star formation rate (SFR) surface density Σ_{SFR} (Section 6.5.2). The exponent in the relation is a key ingredient in the model of [Wang & Lilly \(2022\)](#), which aims to explain the origin of the exponential profiles of the disks of star-forming galaxies. In that model, radial gas inflow in the disk is driven by the Maxwell stress, which depends on the magnetic field strength, which is in turn linked to the gas surface density Σ through the star formation law governing the relation between Σ and Σ_{SFR} .

Corresponding author: Luke Chamandy
lchamandy@niser.ac.in

¹ Scaling relations are relations of the form $X \propto x^a y^b z^c \dots$, where X is a quantity of interest, x , y and z are observable quantities, and a , b and c are constants.

Furthermore, magnetic fields can be used as tracers of physical processes like star formation. Consider that the scaling relation between B and Σ_{SFR} is also useful for modeling the infrared-radio correlation of star-forming galaxies (Schober et al. 2023, and references therein). Here, radio emission is dominated by synchrotron and far infrared by thermal emission from dust. A physical link is provided by star formation, which leads to the cosmic ray electrons involved in synchrotron and the heating of the dust.

While empirical scaling relations can be used directly in physical models, a truly self-consistent model requires such relations to be derived using physical arguments. This is one of the key motivations for the present work.

The paper is organized as follows. Section 2 presents an overview of the model. Then we present each part of the model separately: the magnetic field in Section 3, the turbulence parameters in Section 4, and the remaining relevant quantities in Section 5. In Section 6 we show how solutions can be approximated as scaling relations, and compare these to observations and numerical simulations. Finally, we summarize our results and provide conclusions in Section 7.

2. OVERVIEW OF THE MODEL

The model combines existing analytic solutions for the mean magnetic field (Chamandy et al. 2014) and parameters of the supernova-driven interstellar turbulence (Chamandy & Shukurov 2020). Those solutions have been tested against asymptotic and numerical solutions in the case of mean-field dynamo models (Chamandy et al. 2014; Chamandy 2016; Chamandy et al. 2016), and against direct numerical simulations of the local interstellar medium in the case of turbulence models (Hollins et al. 2017). Furthermore, local galactic dynamo simulations that solve the full equations of MHD are reasonably consistent with dynamo theory (Gressel et al. 2008b,a; Gent et al. 2023, 2024). In addition to our mean-field dynamo and interstellar turbulence models, we use suitably motivated heuristic expressions for quantities like the random magnetic field strength and gas scale height. For simplicity, the gaseous disk is approximated as being comprised of a single-phase fluid in a statistical steady state. We use cylindrical polar coordinates (r, ϕ, z) with the z -axis aligned with the galaxy's rotation axis and $z = 0$ at the galactic midplane. All variables depend on the galactocentric radius r and represent vertical and azimuthal averages over the gaseous galactic disk (although we discuss the azimuthal variations in connection with the effects of the spiral arms).

The model is summarized in Fig. 1. The observables on which the turbulence and magnetic field properties depend are the angular speed of the gas rotation about the galactic centre $\Omega(r)$, the dimensionless rotational velocity shear rate

$$q \equiv -\frac{d \ln \Omega}{d \ln r}, \quad (1)$$

the stellar surface mass density $\Sigma_{\star}(r)$, the gas surface mass density $\Sigma(r)$, the surface density of the SFR $\Sigma_{\text{SFR}}(r)$ and the gas temperature $T(r)$. Note that $q > 0$ since $d\Omega/dr < 0$ in most parts of galaxies, and $q = 1$ for a flat (constant circular velocity) rotation curve. These input quantities – with the exception of $\Omega(r)$ and $q(r)$ – are first used to calculate the gas scale height $h(r)$, the gas density $\rho(r)$, the supernova (SN) rate density $\nu(r)$, the root-mean-square (rms) turbulent velocity $u(r)$, the turbulent correlation length $l(r)$ and turbulent correlation time $\tau(r)$. These quantities are, in turn, used as input for the magnetic field model, along with $\Omega(r)$ and $q(r)$. The magnetic field parameters include the rms strength of the random (turbulent) magnetic field $b(r)$, its degree of anisotropy (defined below), the strength $\bar{B}(r)$ of the mean magnetic field, and its pitch angle

$$\tan p_B(r) = \frac{\bar{B}_r(r)}{\bar{B}_\phi(r)}, \quad (2)$$

where $-\pi/2 < p_B \leq \pi/2$.

The key quantities in the model are defined and summarized in Table 1. Source code has been provided for quickly obtaining scaling relations in various asymptotic limits, including but not limited to the ones presented in Section 6.² In Paper II, we will apply our model to specific galaxies. For this purpose, we will solve the general equations using semi-analytic methods.³

3. MAGNETIC FIELD MODEL

Dynamo amplification is fast enough that the magnetic fields of nearby galaxies (definitely their random components and, likely, their large-scale components, at least in the central parts of galaxies) are expected to be in a saturated state (Beck et al. 1994; Rodrigues et al. 2019). In this statistically steady state, they are predicted to have magnetic energy density similar to the turbulent kinetic energy density and this is borne out in observations (Beck et al. 2019). Thus, in this work we consider only the saturated state of the magnetic field. We separate the field into two main components, the mean field $\bar{\mathbf{B}}$ and the random field \mathbf{b} , so that we may write the total field as

$$\mathbf{B} = \bar{\mathbf{B}} + \mathbf{b}, \quad (3)$$

where overbar represents a suitable averaging (spatial in the case of observed variables and ensemble averages in theoretical results). This separation is both physically and mathematically appropriate because the two terms in equation (3) are believed to be governed by distinct physical processes and are sensitive to different parameters (e.g., Brandenburg

² See <https://github.com/Rnazx/Scaling-Relations>.

³ The source code is available at <https://github.com/Rnazx/goblin>.

Table 1. Key quantities in the model. Adjustable parameters are either fixed at the value in the table, or, as in the case of ψ , allowed to vary within a small range between galaxies but not within them.

Type	Symbol	Quantity	Typical units or value	Reference
Observable	d	Galaxy distance	Mpc	Measured
"	\tilde{r}	Galactocentric radius (angular)	'	"
"	$V_c(r)$	Circular speed	km s^{-1}	"
"	$\Sigma(r)$	Gas surface mass density	$M_\odot \text{kpc}^{-2}$	"
"	$\Sigma_\star(r)$ or $\Sigma_{\text{tot}}(r)$	Stellar or total mass surface density	$M_\odot \text{kpc}^{-2}$	"
"	$\Sigma_{\text{SFR}}(r)$	Star formation rate surface density	$M_\odot \text{yr}^{-1} \text{kpc}^{-2}$	"
"	$T(r)$	Gas temperature	K	"
Derived Observable	r	Galactocentric radius	kpc	$\tilde{r}d$
"	$\Omega(r)$	Gas galactocentric angular speed	$\text{km s}^{-1} \text{kpc}^{-1}$	$\Omega = V_c/r$
"	$q(r)$	Radial shear parameter	–	$q \equiv -d \ln \Omega / d \ln r$
Modelled	$\varepsilon(r)$	Degree of anisotropy of random magnetic field	–	Eq. (8)
"	$b_{\text{ani}}(r)$	Anisotropic random magnetic field strength	μG	Eq. (9) or Eq. (A2)
"	$b_{\text{iso}}(r)$	Isotropic random magnetic field strength	μG	Eq. (10)
"	$B_{\text{eq}}(r)$	Equipartition field strength	g cm^{-3}	Eq. (12)
"	$\bar{B}(r)$	Mean magnetic field strength	μG	Eq. (13) or Eq. (A3)
"	D_c	Critical dynamo number	–	Eq. (14) or Eq. (A5)
"	$D(r)$	Dynamo number	–	Eq. (15)
"	$\eta(r)$	Turbulent diffusivity of \bar{B}	$\text{cm}^2 \text{s}^{-1}$	Eq. (18)
"	$\alpha_m(r)$	α effect term from nonlinear backreaction	km s^{-1}	Eq. (19)
"	$\alpha_k(r)$	α effect in kinematic regime	km s^{-1}	Eq. (20)
"	$p_B(r)$	Mean magnetic field pitch angle	$^\circ$	Eq. (21) or Eq. (A7)
"	$l(r)$	Turbulent correlation length scale	kpc	Eq. (22) or Eq. (A10)
"	$l_{\text{SN}}(r)$	Driving scale of turbulence by isolated SNe	kpc	Eq. (23)
"	$n(r)$	Ambient gas number density	cm^{-3}	Eq. (24)
"	$u(r)$	Root-mean-square turbulent velocity	km s^{-1}	Eq. (25) or Eq. (A16)
"	$\tau(r)$	Turbulent correlation time	Myr	Eq. (26)
"	$\tau_e(r)$	Turnover time of energy-carrying eddies	Myr	Eq. (27)
"	$\tau_r(r)$	Renovation time of turbulence	Myr	Eq. (28) or Eq. (A17)
"	$\nu(r)$	SN rate per unit volume	$\text{kpc}^{-3} \text{Myr}^{-1}$	Eq. (29)
"	$\rho(r)$	Gas mass density	g cm^{-3}	Eq. (30)
"	$c_s(r)$	Sound speed	km s^{-1}	Eq. (31)
"	$\mathcal{M}(r)$	Turbulent sonic Mach number u/c_s	–	Eq. (11)
"	$h(r)$	Gas scale height	kpc	Eq. (32)
Constant	ξ_0	Ratio $b_{\text{iso}}^2/B_{\text{eq}}^2$ for $\mathcal{M} \leq A_1$	0.4	Eq. (10)
"	A_1	Value of \mathcal{M} above which b_{iso} reduces	$\sqrt{2}$	Eq. (10)
"	R_κ	Ratio κ/η of turbulent diffusivity of α_m to that of \bar{B}	0.3	Eq. (13) or (A3)
"	C'_α	Coefficient that sets α_k ceiling	1	Eq. (20)
"	C_l	Constant from turbulence theory	3/4	Eq. (22) or (A10)
"	Γ	Turbulence spectral index	5/3	Eq. (22) or (A10)
"	E_{SN}	Initial SN energy	10^{51}erg	Eq. (23)
"	δ	Fraction of stars that evolve to SNe	8×10^{-3}	Eq. (29)
"	m_\star	Average stellar mass	$0.85 M_\odot$	Eq. (29)
"	A_2	Sets relative strength of thermal pressure term	$\sqrt{2}$	Eq. (33)
"	N	Exponent in Kennicutt-Schmidt law	1.4	Eq. (38)
Adjustable parameter	β	Multiplies magnetic field strengths	–	Eq. (12)
"	K	Normalization factor for \bar{B}	–	Eq. (13) or (A3)
"	C_α	Numerical coefficient of α_k effect	–	Eq. (20)
"	ψ	Multiplies the isolated SN driving scale	–	Eq. (23)
"	ζ	Factor in expression for gas scale height	–	Eq. (32)

& Subramanian 2005; Shukurov & Subramanian 2021), and also because they have distinct observational signatures.

3.1. Random field

Magnetic fields in galaxies are inferred from observations to usually be dominated by a random small-scale component (Beck et al. 2019). Such random fields can be produced by fluctuation (small-scale) dynamo action, as well as the turbulent tangling of the mean magnetic field. It is also possible that part of the random component detected in observations is actually unresolved mean field. Below we neglect the influence of the mean field on the random field for simplicity, leaving such effects for future study.

Random galactic fields are inferred from observations to be anisotropic (e.g. Fletcher et al. 2011). Below, we assume that this anisotropy is solely produced by the large-scale galactic shear arising from differential rotation. Other sources of anisotropy, such as shear and compression in spiral density waves, could also be important. The galactic differential rotation stretches the radial component of the random field, leading to a linear increase with time of the azimuthal component. This can lead to a cumulative effect for a duration of about the correlation time of turbulence τ . Let the standard deviation of any component of the random field be given by $\sigma_i = \sqrt{b_i^2}$, with $i = (r, \phi, z)$. For a random magnetic field in a statistically steady (saturated) state, we can estimate (Shukurov & Subramanian 2021, §4.4.1)

$$\sigma_\phi = \sigma_r(1 + q\Omega\tau). \quad (4)$$

Galactic outflows (winds or fountain flow) may also contain large-scale shear, which would enhance σ_z relative to σ_r . We neglect galactic outflows for simplicity, but general expressions that include the mean vertical outflow speed U_0 are given in Appendix A.1. With $U_0 = 0$, we obtain

$$\sigma_z = \sigma_r. \quad (5)$$

The strength of the random field is thus given by

$$b \equiv \sqrt{b^2} = \sqrt{\sigma_r^2 + \sigma_\phi^2 + \sigma_z^2} = \sigma_r \sqrt{2 + (1 + q\Omega\tau)^2} \quad (6)$$

and that of the isotropic background by

$$b_{\text{iso}} = \sqrt{3}\sigma_r. \quad (7)$$

The degree of anisotropy can be expressed as

$$\varepsilon = \frac{b_{\text{ani}}}{b}, \quad (8)$$

where

$$b_{\text{ani}} \equiv \sqrt{b^2 - b_{\text{iso}}^2} = \frac{b_{\text{iso}}}{\sqrt{3}} \left[2q\Omega\tau \left(1 + \frac{q\Omega\tau}{2} \right) \right]^{1/2}. \quad (9)$$

Simulations of fluctuation dynamos in periodic boxes with isotropic forcing can be used to estimate the strength of the random field in the saturated state. Since large-scale shear is typically not included in such simulations, they are best used to estimate b_{iso} , rather than b . In particular, they can help to constrain the ratio ξ of energy density of the saturated magnetic field $b_{\text{iso}}^2/8\pi$ to that of the turbulent motions $\frac{1}{2}\rho u^2$, for a range of magnetic Reynolds and magnetic Prandtl numbers; in galaxies, one expects $\text{Rm} \gg 1$ and $\text{Pm} \gg 1$. These simulations suggest that $\xi = b_{\text{iso}}^2/4\pi\rho u^2$ ranges from ≈ 0.4 for solenoidally forced subsonic turbulence, to values that are considerably smaller for compressively forced or supersonic turbulence. Based loosely on results from Federrath et al. (2011) (see also Seta & Federrath 2021) we choose

$$b_{\text{iso}} = \frac{\xi_0^{1/2} B_{\text{eq}}}{\max(1, \mathcal{M}/A_1)}, \quad (10)$$

where A_1 is constant of order unity,

$$\mathcal{M} \equiv \frac{u}{c_s} \quad (11)$$

is the turbulent sonic Mach number, c_s is the speed of sound and $\xi_0 = 0.4$. Here,

$$B_{\text{eq}} = \beta(4\pi\rho)^{1/2}u \quad (12)$$

is the field strength corresponding to energy equipartition with turbulence. A parameter, β , has been inserted to account for imprecision in both theory and observational inference.

3.2. Mean field

Spiral galaxies also contain magnetic field components that are coherent on scales up to the system size. This large-scale component (sometimes called the mean or regular field) can generally be explained by appealing to mean-field dynamo action (Beck et al. 2019). Below we apply α - Ω dynamo theory including a nonlinear backreaction that quenches the dynamo and leads to saturation (Pouquet et al. 1976; Krause & Rädler 1980; Kleeorin & Ruzmaikin 1982; Ruzmaikin et al. 1988; Blackman & Field 2002; Rädler et al. 2003; Brandenburg & Subramanian 2005; Shukurov et al. 2006; Subramanian & Brandenburg 2006; Sur et al. 2007; Chamandy et al. 2014; Gopalakrishnan & Subramanian 2023).

We make use of an analytic steady-state solution of the mean-field dynamo equations that assumes a thin disc and employs the no- z approximation to replace z -derivatives by divisions by $h(r)$, with coefficients chosen to produce good agreement with solutions that retain the z -dependence (Subramanian & Mestel 1993; Moss 1995; Phillips 2001; Chamandy et al. 2014). General expressions that allow for a finite mean vertical velocity are derived in Chamandy et al. (2014) and can be found in Section A.1. In the absence of mean

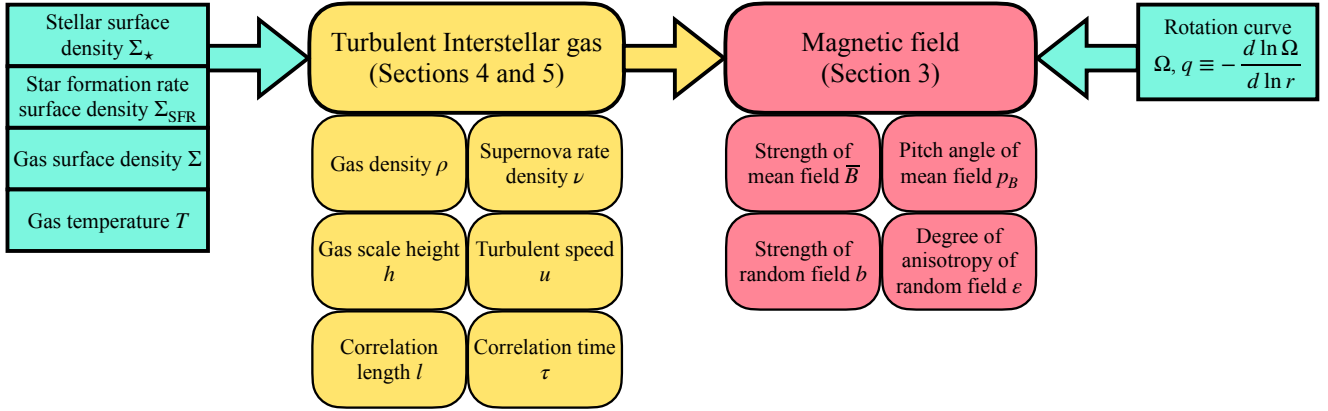


Figure 1. The structure of the model showing, with reference to various parts of the text, the hierarchy of input and derived parameters.

vertical outflow or inflow, the strength of the mean magnetic field in the saturated state is given by

$$\bar{B} \equiv |\bar{\mathbf{B}}| = K \frac{\pi l}{h} \left[\left(\frac{D}{D_c} - 1 \right) R_\kappa \right]^{1/2} B_{\text{eq}}, \quad (13)$$

where K is a factor of order 0.1–1 that accounts for theoretical uncertainty (Chamandy & Singh 2018), D is the dynamo number, subscripts ‘k’ and ‘c’ refer to the kinematic ($\bar{B} \ll B_{\text{eq}}$) and critical (no growth or decay) values, and $D > D_c$ (supercritical dynamo); if $D \leq D_c$ then we instead adopt $\bar{B} = 0$. The critical dynamo number is given by

$$D_c = - \left(\frac{\pi}{2} \right)^5, \quad (14)$$

and the kinematic dynamo number by

$$D = R_\alpha R_\Omega, \quad (15)$$

with Reynolds-type dimensionless numbers

$$R_\alpha \equiv \frac{\alpha_k h}{\eta}, \quad R_\Omega \equiv - \frac{q \Omega h^2}{\eta}, \quad R_\kappa \equiv \frac{\kappa}{\eta}. \quad (16)$$

where

$$\alpha_k = - \frac{1}{3} \tau \mathbf{u} \cdot \nabla \times \mathbf{u}, \quad (17)$$

the turbulent diffusivity of $\bar{\mathbf{B}}$ is given by

$$\eta = \frac{1}{3} \tau u^2, \quad (18)$$

and κ is the turbulent diffusivity of the quantity

$$\alpha_m = \frac{1}{3} \tau \frac{\overline{\mathbf{b} \cdot \nabla \times \mathbf{b}}}{4\pi\rho}, \quad (19)$$

which becomes important in the nonlinear regime owing to the backreaction of the field onto the flow. The total contribution

to the α effect is obtained by summing α_k and α_m . We approximate α_k as (Ruzmaikin et al. 1988; Chamandy et al. 2016)

$$\alpha_k = \begin{cases} \frac{C_\alpha \tau^2 u^2 \Omega}{h}, & \text{if } \min \left(1, \frac{C'_\alpha h}{C_\alpha \tau u} \right) \geq \Omega \tau; \\ \frac{C_\alpha \tau u^2}{h}, & \text{if } \min \left(\Omega \tau, \frac{C'_\alpha h}{C_\alpha \tau u} \right) \geq 1; \\ C'_\alpha u, & \text{if } \min (\Omega \tau, 1) \geq \frac{C'_\alpha h}{C_\alpha \tau u}, \end{cases} \quad (20)$$

where C_α and C'_α are constants of order unity that account for a lack of precision in the modeling; note that $C'_\alpha u$ acts as a ceiling on α_k . The pitch angle of $\bar{\mathbf{B}}$ is given by

$$\tan p_B = \frac{\bar{B}_r}{\bar{B}_\phi} = \frac{\pi^2}{4R_\Omega} = - \frac{\pi^2 \tau u^2}{12 q \Omega h^2}, \quad (21)$$

defined such that $-\pi/2 < p_B \leq \pi/2$ with $p_B < 0$ for trailing spirals (with respect to the galactic rotation).

4. INTERSTELLAR TURBULENCE MODEL

Magnetic field solutions depend on the rms turbulent velocity u , the turbulent correlation time τ and length l , which are either very challenging (u and l) or impossible (τ) to measure directly from observations. The quantity u can be inferred from the line-of-sight velocity dispersion, which is commonly observed in galaxies, but the data is contaminated by contributions from thermal motions, cloud motions, and outflows, which are difficult to separate out (e.g. Mogotsi et al. 2016).⁴ Therefore, we seek solutions for these turbulence quantities in terms of accessible observable quantities.

Supernova (SN) feedback is generally believed to be the dominant driver of turbulence in nearby galaxies (e.g. Klessen

⁴ See Burkhardt 2021 for a review of methods to study interstellar turbulence using observations.

& Glover 2016; Krumholz et al. 2018; Bacchini et al. 2020). For SN-driven turbulence, u , τ and l have been estimated using an analytic model that considers turbulence to be simultaneously driven by isolated SNe and superbubbles (SBs) formed by multiple SNe in OB associations (Chamandy & Shukurov 2020). In the model, a fraction f_{SB} of SNe are assumed to contribute to SBs. Here we neglect SBs by setting $f_{\text{SB}} = 0$, but we include a summary of the general model ($f_{\text{SB}} \neq 0$) in Appendix A.2.

4.1. Correlation length

For $f_{\text{SB}} = 0$, equation (A10) for the turbulent correlation length becomes

$$l = \left(\frac{\Gamma - 1}{\Gamma} \right) C_l l_{\text{SN}} = \frac{3}{10} l_{\text{SN}}, \quad (22)$$

where we have assumed $\Gamma = 5/3$ and $C_l = 3/4$ (see Section A.2.1 and Table 1), and where l_{SN} is the driving scale of turbulence driven by isolated SNe. The quantity l_{SN} is equal to the radius of the SN remnant (SNR) when its age is t_s^{SN} , defined as the time at which the SNR expansion speed becomes equal to the ambient sound speed, $\dot{R}_{\text{SN}} = c_s$. At this time the SNR is assumed to fragment and merge with the interstellar medium (ISM), transferring its energy to the latter. This gives

$$l_{\text{SN}} = R_{\text{SN}}(t_s^{\text{SN}}) = 0.14 \text{ kpc } \psi E_{51}^{16/51} n_{0.1}^{-19/51} c_{10}^{-1/3}, \quad (23)$$

where $E_{51} = E_{\text{SN}}/10^{51} \text{ erg}$ is the SN energy (excluding that in neutrinos), $n_{0.1} = n/0.1 \text{ cm}^{-3}$ is the gas number density, and $c_{10} = c_s/10 \text{ km s}^{-1}$. A dimensionless parameter of order unity, ψ , is introduced in the present work to account for the uncertainty in the model. To convert from mass density to number density, we have used the expression

$$n = \frac{\rho}{\mu m_{\text{H}}}, \quad (24)$$

with mean molecular mass $\mu = 14/11$.

4.2. Root-mean-square turbulent velocity

The rms turbulent velocity, u , is estimated by equating the energy injection rate per unit volume from SNe with the dissipation rate per unit volume $\sim \rho u^3/2l$ owing to the turbulent energy cascade. With $f_{\text{SB}} = 0$, equation (A16) becomes

$$u = \left(\frac{4\pi}{3} l_{\text{SN}}^3 l c_s^2 v \right)^{1/3}, \quad (25)$$

with l given by equation (22) and l_{SN} by equation (23).

4.3. Correlation time

We estimate the correlation time τ as the minimum of the turnover time τ_e of energy-carrying eddies, and the time τ_r for the flow to renovate due to the passage of an SN blast wave,

$$\tau = \min(\tau_r, \tau_e). \quad (26)$$

The eddy turnover time (comparable to the lifetime of the largest eddies) is estimated as

$$\tau_e = \frac{l}{u}, \quad (27)$$

where l is given by equation (22) and u is given by equation (25) for the case $f_{\text{SB}} = 0$. For this case, the renovation time is given by

$$\tau_r = \tau_{\text{SN}}^r = \frac{3}{4\pi l_{\text{SN}}^3 v} = 6.8 \text{ Myr } \frac{1}{4} v_{50}^{-1} E_{51}^{-16/17} n_{0.1}^{19/17} c_{10}. \quad (28)$$

Equations (22) (or A10), (25) (or A16) and (26), can be used wherever the quantities l , u and τ appear in the equations of Section 3.

5. FORMULATING THE EQUATIONS IN TERMS OF THE OBSERVABLES

We must still obtain expressions for the SN rate per unit volume $\nu(r)$, gas density $\rho(r)$, disk scale height $h(r)$ and sound speed $c_s(r)$ in terms of the observable quantities.

Following Van Eck et al. (2015), we write

$$\nu = \frac{\delta \Sigma_{\text{SFR}}}{2hm_{\star}} \quad (29)$$

where $\Sigma_{\text{SFR}}/2h$ is the mean SFR volume density averaged across the gas disk, $\delta \approx 8 \times 10^{-3}$ is the fraction of stars that evolve to SNe for the initial mass function (IMF) of Kroupa (2008), and $m_{\star} = 0.85 M_{\odot}$ is the average stellar mass for this IMF (other choices of IMF would lead to small changes in δ and m_{\star}).

For an exponential or uniform density disk of scale height or half-thickness h , we have

$$\rho = \frac{\Sigma}{2h}. \quad (30)$$

Approximating the ISM as a uniform ideal gas, we write the sound speed as

$$c_s = \left(\frac{\gamma k_{\text{B}} T}{\mu m_{\text{H}}} \right)^{1/2}. \quad (31)$$

A reasonable choice for the adiabatic index is $\gamma = 1.5$ (Vandenbroucke et al. 2013).

The scale height h can be estimated from vertical hydrostatic balance (e.g. Rodrigues et al. 2019). We use

$$h \approx \frac{w^2}{3\pi G(\Sigma + \Sigma_{\star}/\zeta)} \approx \zeta \frac{w^2}{3\pi G \Sigma_{\text{tot}}}, \quad (32)$$

where

$$w \equiv (u^2 + A_2^2 c_s^2)^{1/2}. \quad (33)$$

Here $A_2^2 = 2$ for $\gamma = 3/2$, Σ_{\star} is the surface density of stars, σ_{\star} is the 1D velocity dispersion of stars, ζ (formally equal to

Table 2. Versions of the model for which scaling relations are derived. See Section 6.1 for details.

Model	Driving scale	Regime	Correl. time	Mach no.
S	$\propto R_{\text{SN}}(t_s)$	a	$\tau_e < \tau_r \Rightarrow \tau = \tau_e$	$\mathcal{M} \ll A$
		b	$\tau_e < \tau_r \Rightarrow \tau = \tau_e$	$\mathcal{M} \gg A$
		c	$\tau_r < \tau_e \Rightarrow \tau = \tau_r$	$\mathcal{M} \ll A$
		d	$\tau_r < \tau_e \Rightarrow \tau = \tau_r$	$\mathcal{M} \gg A$
Alt1	$\propto h$		$\tau = \tau_e$	$\mathcal{M} = \text{const}$
Alt2	$\propto h$	a	$\tau = \tau_e$	$\mathcal{M} \ll A$
		b	$\tau = \tau_e$	$\mathcal{M} \gg A$

$\sqrt{3}\sigma_{\star}/w$ above) is a parameter that allows for uncertainty in the model, and the last equality of (32) assumes that $\Sigma_{\star}/\zeta \gg \Sigma$ and that stars dominate the total surface density of the disk Σ_{tot} , which includes stars, gas and dark matter.⁵ A similar expression – but with u^2 replacing w^2 – is motivated in Forbes et al. (2012).⁶ Equation (32) is a generalization of their formula that includes the thermal pressure, $P_{\text{thm}} = \rho c_s^2/\gamma \approx \frac{2}{3}\rho c_s^2$ (if $\gamma = 3/2$), in addition to the turbulent pressure $P_{\text{tur}} = \frac{1}{3}\rho u^2$.⁷

The equations of Sections 3, 4 and 5 can be used to calculate the vertically and azimuthally averaged turbulence and magnetic field properties at a radius r , in terms of commonly observed quantities.

6. SCALING RELATIONS

We now derive scaling relations for key turbulence and magnetic quantities. These can be obtained using straightforward algebra, but we have provided the link to a tool which facilitates this in Section 2. We focus on the power law exponents, but a sample calculation of the proportionality coefficients is provided in Sec. 6.7. Adjustable parameters ζ , ψ , C_{α} , K and β are assumed to be constant or to vary weakly between galaxies, so the exponents do not depend on them. We set $A_1 = A_2 \equiv A$ for simplicity and restrict our analysis to the asymptotic cases $\mathcal{M} \ll A$ and $\mathcal{M} \gg A$, so that w can be replaced, respectively, by c_s or u in equation (32), but we comment on the regime $\mathcal{M} \approx A$ in Section 6.4.

To obtain scaling relations for b_{ani} and \bar{B} , additional approximations are necessary. In equation (9) for b_{ani} , we assume

⁵ In practice, we only require that $\Sigma_{\text{tot}} \propto \Sigma_{\star}$, since ζ can be rescaled.

⁶ See also the expression for the total midplane pressure in Elmegreen 1989, which would lead to a similar expression for the scale height to that of Forbes et al. (2012).

⁷ For example, naively comparing stellar velocity dispersion data (Mogotsi & Romeo 2019) with gas velocity dispersion data (Mogotsi et al. 2016) for two different sets of galaxies suggests a mean ratio of stellar to gas 1D velocity dispersions in the range 5–10.

that $q\Omega\tau/2 \ll 1$. This condition is likely satisfied in the Solar Neighbourhood, for example, where $q\Omega\tau \approx 0.14$ assuming $\Omega = 27.5 \text{ km s}^{-1} \text{ kpc}^{-1}$, $q = 1$ and $\tau = 5 \text{ Myr}$ (Hollins et al. 2017; Chamandy & Shukurov 2020). Equation (9) then simplifies to

$$b_{\text{ani}} = \left(\frac{2}{3}q\Omega\tau\right)^{1/2} b_{\text{iso}}, \quad (34)$$

where b_{iso} is still given by equation (10).

In order to be able to write down a scaling relation for \bar{B} , we assume $\min(1, C'_{\alpha}h/C_{\alpha}\tau u) \geq \Omega\tau$, so that, from equation (20) we have the standard result (Krause & Rädler 1980; Ruzmaikin et al. 1988)

$$\alpha_k = \frac{C_{\alpha}\tau^2 u^2 \Omega}{h}. \quad (35)$$

In addition, we assume that the dynamo is highly supercritical, i.e. $D/D_c \gg 1$. This assumption is generally satisfied in the inner parts of galaxies. With these assumptions, equation (13) simplifies to

$$\bar{B} = K \frac{\pi l}{h} \left(\frac{DR_{\kappa}}{D_c}\right)^{1/2} B_{\text{eq}}, \quad (36)$$

with

$$D = -\frac{9C_{\alpha}qh^2\Omega^2}{u^2}, \quad (37)$$

where we have made use of equations (15), (16), (18) and (35). Note that $D \propto q\Omega^2$, so there is some tension between assuming both $D \gg D_c$ and $q\Omega\tau/2 \ll 1$. Both assumptions may be satisfied simultaneously for small τ . Upon substituting equations (37) and (12) in equation (36), we find that $\bar{B} \propto l\Omega(C_{\alpha}q\rho R_{\kappa})^{1/2}$. Simulations suggest $R_{\kappa} \approx 0.3$ (Mitra et al. 2010), while a recent analytic calculation gives $R_{\kappa} = 21(1 + \tilde{\xi})/27$ with $\tilde{\xi} = b^2/B_{\text{eq}}^2$ (Gopalakrishnan & Subramanian 2023). In the present work, R_{κ} is assumed to be constant.

We now have all of the expressions needed to obtain scaling relations for $h(r)$, $u(r)$, $l(r)$, $\tau(r)$, $b_{\text{iso}}(r)$, $b_{\text{ani}}(r)$, $\bar{B}(r)$ and $p_B(r)$ in terms of the observables $\Sigma_{\star}(r)$ or $\Sigma_{\text{tot}}(r)$, $\Sigma(r)$, $\Sigma_{\text{SFR}}(r)$, $\Omega(r)$, $q(r)$ and $T(r)$. However, the scaling relations will depend on whether $\tau_e > \tau_r$ or $\tau_e < \tau_r$ (equation 26), and on whether $u \ll Ac_s$ or $u \gg Ac_s$ (equation 33). For transonic turbulence we might expect scaling relation exponents in between those for the subsonic and supersonic cases.

6.1. Alternative turbulence models

Turbulence driving in galaxies is still not very well-understood and there is still a lack of consensus, e.g., about the driving scale(s). Thus, we choose to explore the implications of making different assumptions about turbulence driving, as summarized in Table 2. Model S is our fiducial model and uses the framework summarized above for turbulence driven by expanding isolated SNRs. We include two simpler models

Table 3. Predicted scaling relations for parameters h , l , u and τ for our fiducial SN-driven turbulence model (Model S) as well as two simpler alternative models Alt1 and Alt2. To derive scaling relations, the models are subdivided into the asymptotic regimes $\mathcal{M} \ll A$ and $\mathcal{M} \gg A$ as well as $\tau_e/\tau_l < 1$ and $\tau_e/\tau_l > 1$. See Section 6 for details.

Model	$h \propto$	$l \propto$	$u \propto$	$\tau \propto$
Sa	$\Sigma_{\text{tot}}^{-1} T$	$\Sigma_{\text{tot}}^{-0.37} \Sigma_{\text{SFR}}^{-0.37} T^{0.21}$	$\Sigma_{\text{tot}}^{-0.50} \Sigma_{\text{SFR}}^{-0.16} \Sigma_{\text{SFR}}^{1/3} T^{0.27}$	$\Sigma_{\text{tot}}^{-0.12} \Sigma_{\text{SFR}}^{-0.21} \Sigma_{\text{SFR}}^{-1/3} T^{-0.07}$
Sb	$\Sigma_{\text{tot}}^{-1.48} \Sigma_{\text{SFR}}^{-1.49} \Sigma_{\text{SFR}}^{0.99} T^{0.33}$	$\Sigma_{\text{tot}}^{-0.92} \Sigma_{\text{SFR}}^{-0.55} \Sigma_{\text{SFR}}^{0.37} T^{-0.04}$	$\Sigma_{\text{tot}}^{-0.74} \Sigma_{\text{SFR}}^{-0.24} \Sigma_{\text{SFR}}^{0.50} T^{0.17}$	$\Sigma_{\text{SFR}}^{-0.18} \Sigma_{\text{tot}}^{-0.31} \Sigma_{\text{SFR}}^{-0.13} T^{-0.21}$
Sc	$\Sigma_{\text{tot}}^{-1} T$	$\Sigma_{\text{tot}}^{-0.37} \Sigma_{\text{SFR}}^{-0.37} T^{0.21}$	$\Sigma_{\text{tot}}^{-0.50} \Sigma_{\text{SFR}}^{-0.16} \Sigma_{\text{SFR}}^{1/3} T^{0.27}$	$\Sigma_{\text{SFR}}^{19/17} \Sigma_{\text{tot}}^{2/17} \Sigma_{\text{SFR}}^{-1} T^{13/34}$
Sd	$\Sigma_{\text{tot}}^{-1.48} \Sigma_{\text{SFR}}^{-1.49} \Sigma_{\text{SFR}}^{0.99} T^{0.33}$	$\Sigma_{\text{tot}}^{-0.92} \Sigma_{\text{SFR}}^{-0.55} \Sigma_{\text{SFR}}^{0.37} T^{-0.04}$	$\Sigma_{\text{tot}}^{-0.74} \Sigma_{\text{SFR}}^{-0.24} \Sigma_{\text{SFR}}^{0.50} T^{0.17}$	$\Sigma_{\text{SFR}}^{1.29} \Sigma_{\text{tot}}^{0.17} \Sigma_{\text{SFR}}^{-1.12} T^{0.46}$
Alt1	$\Sigma_{\text{tot}}^{-1} T$	$\Sigma_{\text{tot}}^{-1} T$	$T^{1/2}$	$\Sigma_{\text{tot}}^{-1} T^{1/2}$
Alt2a	$\Sigma_{\text{tot}}^{-1} T$	$\Sigma_{\text{tot}}^{-1} T$	$\Sigma_{\text{SFR}}^{-1} \Sigma_{\text{SFR}}^{1/3} T^{4/3}$	$\Sigma_{\text{SFR}}^{-1/3} T^{-1/3}$
Alt2b	$\Sigma_{\text{tot}} \Sigma_{\text{SFR}}^{-2/3} T^{-2/3}$	$\Sigma_{\text{tot}} \Sigma_{\text{SFR}}^{-2/3} T^{-2/3}$	$\Sigma_{\text{tot}} \Sigma_{\text{SFR}}^{-1/3} T^{-1/3}$	$\Sigma_{\text{SFR}}^{-1/3} T^{-1/3}$

Table 4. Predicted scaling relations for the strengths of the isotropic (b_{iso}) and anisotropic (b_{ani}) components of the random magnetic field, and the strength (\bar{B}) and pitch angle (p_B) of the mean magnetic field. Expressions for b_{ani} assume $q\Omega\tau/2 \ll 1$ and those for \bar{B} assume $\min(1, C'_\alpha h/C_\alpha \tau u) \geq \Omega\tau$ and $D \gg D_c$.

Model	$b_{\text{iso}} \propto$	$b_{\text{ani}} \propto$	$\bar{B} \propto$	$\tan p_B \propto$
Sa	$\Sigma_{\text{tot}}^{0.003} \Sigma_{\text{SFR}}^{0.34} \Sigma_{\text{SFR}}^{1/3} T^{-0.23}$	$q^{1/2} \Omega^{1/2} \Sigma_{\text{tot}}^{0.07} \Sigma_{\text{SFR}}^{0.23} \Sigma_{\text{SFR}}^{1/6} T^{-0.26}$	$q^{1/2} \Omega \Sigma_{\text{tot}}^{0.13} \Sigma_{\text{SFR}}^{0.13} T^{-0.29}$	$q^{-1} \Omega^{-1} \Sigma_{\text{tot}}^{-0.87} \Sigma_{\text{SFR}}^{1.46} \Sigma_{\text{SFR}}^{1/3} T^{-1.52}$
Sb	$\Sigma_{\text{tot}}^{1.24} \Sigma_{\text{SFR}}^{0.74} \Sigma_{\text{SFR}}^{-0.50} T^{0.33}$	$q^{1/2} \Omega^{1/2} \Sigma_{\text{tot}}^{1.15} \Sigma_{\text{SFR}}^{0.59} \Sigma_{\text{SFR}}^{-0.56} T^{0.23}$	$q^{1/2} \Omega \Sigma_{\text{tot}}^{0.32} \Sigma_{\text{SFR}}^{0.19} \Sigma_{\text{SFR}}^{-0.13} T^{-0.21}$	$q^{-1} \Omega^{-1} \Sigma_{\text{tot}}^{1.29} \Sigma_{\text{SFR}}^{2.17} \Sigma_{\text{SFR}}^{-1.12} T^{-0.54}$
Sc	$\Sigma_{\text{tot}}^{0.003} \Sigma_{\text{SFR}}^{0.34} \Sigma_{\text{SFR}}^{1/3} T^{-0.23}$	$q^{1/2} \Omega^{1/2} \Sigma_{\text{tot}}^{0.56} \Sigma_{\text{SFR}}^{0.40} \Sigma_{\text{SFR}}^{-1/6} T^{-0.03}$	$q^{1/2} \Omega \Sigma_{\text{tot}}^{0.13} \Sigma_{\text{SFR}}^{0.13} T^{-0.29}$	$q^{-1} \Omega^{-1} \Sigma_{\text{tot}}^{0.12} \Sigma_{\text{SFR}}^{1.79} \Sigma_{\text{SFR}}^{-1/3} T^{-1.07}$
Sd	$\Sigma_{\text{tot}}^{1.24} \Sigma_{\text{SFR}}^{0.74} \Sigma_{\text{SFR}}^{-0.50} T^{0.33}$	$q^{1/2} \Omega^{1/2} \Sigma_{\text{tot}}^{1.88} \Sigma_{\text{SFR}}^{0.83} \Sigma_{\text{SFR}}^{-1.05} T^{0.57}$	$q^{1/2} \Omega \Sigma_{\text{tot}}^{0.32} \Sigma_{\text{SFR}}^{0.19} \Sigma_{\text{SFR}}^{-0.13} T^{-0.21}$	$q^{-1} \Omega^{-1} \Sigma_{\text{tot}}^{2.77} \Sigma_{\text{SFR}}^{2.66} \Sigma_{\text{SFR}}^{-2.11} T^{0.13}$
Alt1	$\Sigma_{\text{tot}}^{1/2} \Sigma_{\text{tot}}^{1/2}$	$q^{1/2} \Omega^{1/2} \Sigma_{\text{tot}}^{1/2} T^{1/4}$	$q^{1/2} \Omega \Sigma_{\text{tot}}^{1/2} \Sigma_{\text{tot}}^{-1/2} T^{1/2}$	$q^{-1} \Omega^{-1} \Sigma_{\text{tot}} T^{-1/2}$
Alt2a	$\Sigma_{\text{tot}}^{1/2} \Sigma_{\text{SFR}}^{-1/2} \Sigma_{\text{SFR}}^{1/3} T^{5/6}$	$q^{1/2} \Omega^{1/2} \Sigma_{\text{tot}}^{1/2} \Sigma_{\text{SFR}}^{-1/2} \Sigma_{\text{SFR}}^{1/6} T^{2/3}$	$q^{1/2} \Omega \Sigma_{\text{tot}}^{1/2} \Sigma_{\text{SFR}}^{-1/2} T^{1/2}$	$q^{-1} \Omega^{-1} \Sigma_{\text{SFR}}^{1/3} T^{1/3}$
Alt2b	$\Sigma_{\text{tot}}^{1/2} \Sigma_{\text{SFR}}^{-1/2} \Sigma_{\text{SFR}}^{1/3} T^{5/6}$	$q^{1/2} \Omega^{1/2} \Sigma_{\text{tot}}^{1/2} \Sigma_{\text{SFR}}^{-1/2} \Sigma_{\text{SFR}}^{1/6} T^{2/3}$	$q^{1/2} \Omega \Sigma_{\text{tot}}^{1/2} \Sigma_{\text{SFR}}^{-1/3} T^{-1/3}$	$q^{-1} \Omega^{-1} \Sigma_{\text{SFR}}^{1/3} T^{1/3}$

Table 5. As Table 3, but with the additional assumption that $\Sigma_{\text{SFR}} \propto \Sigma^{1.4}$.

Model	$h \propto$	$l \propto$	$u \propto$	$\tau \propto$
Sa	$\Sigma_{\text{tot}}^{-1} T$	$\Sigma_{\text{tot}}^{-0.37} \Sigma_{\text{SFR}}^{-0.27} T^{0.21}$	$\Sigma_{\text{tot}}^{-0.16} \Sigma_{\text{SFR}}^{-0.021} T^{0.27}$	$\Sigma_{\text{tot}}^{-0.21} \Sigma_{\text{SFR}}^{-0.24} T^{-0.07}$
Sb	$\Sigma_{\text{tot}}^{-1.49} \Sigma_{\text{SFR}}^{-0.064} T^{0.33}$	$\Sigma_{\text{tot}}^{-0.55} \Sigma_{\text{SFR}}^{-0.29} T^{-0.04}$	$\Sigma_{\text{tot}}^{-0.24} \Sigma_{\text{SFR}}^{-0.032} T^{0.17}$	$\Sigma_{\text{tot}}^{-0.31} \Sigma_{\text{SFR}}^{-0.26} T^{-0.21}$
Sc	$\Sigma_{\text{tot}}^{-1} T$	$\Sigma_{\text{tot}}^{-0.37} \Sigma_{\text{SFR}}^{-0.27} T^{0.21}$	$\Sigma_{\text{tot}}^{-0.16} \Sigma_{\text{SFR}}^{-0.021} T^{0.27}$	$\Sigma_{\text{tot}}^{2/17} \Sigma_{\text{SFR}}^{-0.20} T^{13/34}$
Sd	$\Sigma_{\text{tot}}^{-1.49} \Sigma_{\text{SFR}}^{-0.064} T^{0.33}$	$\Sigma_{\text{tot}}^{-0.55} \Sigma_{\text{SFR}}^{-0.29} T^{-0.04}$	$\Sigma_{\text{tot}}^{-0.24} \Sigma_{\text{SFR}}^{-0.032} T^{0.17}$	$\Sigma_{\text{tot}}^{0.17} \Sigma_{\text{SFR}}^{-0.19} T^{0.46}$
Alt1	$\Sigma_{\text{tot}}^{-1} T$	$\Sigma_{\text{tot}}^{-1} T$	$T^{1/2}$	$\Sigma_{\text{tot}}^{-1} T^{1/2}$
Alt2a	$\Sigma_{\text{tot}}^{-1} T$	$\Sigma_{\text{tot}}^{-1} T$	$\Sigma_{\text{SFR}}^{-1} \Sigma_{\text{SFR}}^{1/3} T^{4/3}$	$\Sigma_{\text{SFR}}^{-1/3} T^{-1/3}$
Alt2b	$\Sigma_{\text{tot}} \Sigma_{\text{SFR}}^{-2/3} T^{-2/3}$	$\Sigma_{\text{tot}} \Sigma_{\text{SFR}}^{-2/3} T^{-2/3}$	$\Sigma_{\text{tot}} \Sigma_{\text{SFR}}^{-1/3} T^{-1/3}$	$\Sigma_{\text{SFR}}^{-1/3} T^{-1/3}$

for comparison. Model Alt1 is our minimalistic model, which assumes $l \propto h$, $u \propto c_s$ and $\tau \propto l/u$ (in deriving the scaling relation exponents, equalities can be replaced with proportionalities). Model Alt2 is our hybrid model and assumes $l_{\text{SN}} \propto h$ and $\tau \propto l/u$, but retains equation (25) for u , which permits two asymptotic regimes ($\mathcal{M} \ll A$ and $\mathcal{M} \gg A$), as in Model S. The PYTHON tool mentioned in Section 2 can be used to explore a wider set of combinations of assumptions about turbulence.

6.2. Expressions

Scaling relations for Models S, Alt1 and Alt2 are given in Tables 3 and 4. Where reduced fractional forms of exponents are cumbersome to write, we have rounded to decimal values. We choose to write the scaling relations in terms of Σ_{tot} rather than Σ_* , but we refer to them somewhat interchangeably below. Note that the dependency on ζ is the same as the dependency on $1/\Sigma_{\text{tot}}$.

Table 6. As Table 4, but with the additional assumption that $\Sigma_{\text{SFR}} \propto \Sigma^{1.4}$.

Model	$b_{\text{iso}} \propto$	$b_{\text{ani}} \propto$	$\bar{B} \propto$	$\tan p_B \propto$
Sa	$\Sigma_{\text{tot}}^{0.34} \Sigma_{\text{SFR}}^{0.34} T^{-0.23}$	$q^{1/2} \Omega^{1/2} \Sigma_{\text{tot}}^{0.23} \Sigma_{\text{SFR}}^{0.21} T^{-0.26}$	$q^{1/2} \Omega \Sigma_{\text{tot}}^{0.13} \Sigma_{\text{SFR}}^{0.091} T^{-0.29}$	$q^{-1} \Omega^{-1} \Sigma_{\text{tot}}^{1.46} \Sigma_{\text{SFR}}^{-0.29} T^{-1.52}$
Sb	$\Sigma_{\text{tot}}^{0.74} \Sigma_{\text{SFR}}^{0.39} T^{0.33}$	$q^{1/2} \Omega^{1/2} \Sigma_{\text{tot}}^{0.59} \Sigma_{\text{SFR}}^{0.26} T^{0.23}$	$q^{1/2} \Omega \Sigma_{\text{tot}}^{0.19} \Sigma_{\text{SFR}}^{0.10} T^{-0.21}$	$q^{-1} \Omega^{-1} \Sigma_{\text{tot}}^{2.17} \Sigma_{\text{SFR}}^{-0.19} T^{-0.54}$
Sc	$\Sigma_{\text{tot}}^{0.34} \Sigma_{\text{SFR}}^{0.34} T^{-0.23}$	$q^{1/2} \Omega^{1/2} \Sigma_{\text{tot}}^{0.40} \Sigma_{\text{SFR}}^{0.23} T^{-0.03}$	$q^{1/2} \Omega \Sigma_{\text{tot}}^{0.13} \Sigma_{\text{SFR}}^{0.091} T^{-0.29}$	$q^{-1} \Omega^{-1} \Sigma_{\text{tot}}^{1.79} \Sigma_{\text{SFR}}^{-0.24} T^{-1.07}$
Sd	$\Sigma_{\text{tot}}^{0.74} \Sigma_{\text{SFR}}^{0.39} T^{0.33}$	$q^{1/2} \Omega^{1/2} \Sigma_{\text{tot}}^{0.83} \Sigma_{\text{SFR}}^{0.29} T^{0.57}$	$q^{1/2} \Omega \Sigma_{\text{tot}}^{0.19} \Sigma_{\text{SFR}}^{0.10} T^{-0.21}$	$q^{-1} \Omega^{-1} \Sigma_{\text{tot}}^{2.66} \Sigma_{\text{SFR}}^{-0.13} T^{0.13}$
Alt1	$\Sigma_{\text{tot}}^{1/2} \Sigma_{\text{SFR}}^{0.36}$	$q^{1/2} \Omega^{1/2} \Sigma_{\text{SFR}}^{0.36} T^{1/4}$	$q^{1/2} \Omega \Sigma_{\text{tot}}^{-1/2} \Sigma_{\text{SFR}}^{0.36} T^{1/2}$	$q^{-1} \Omega^{-1} \Sigma_{\text{tot}} T^{-1/2}$
Alt2a	$\Sigma_{\text{tot}}^{-1/2} \Sigma_{\text{SFR}}^{0.69} T^{5/6}$	$q^{1/2} \Omega^{1/2} \Sigma_{\text{tot}}^{-1/2} \Sigma_{\text{SFR}}^{0.52} T^{2/3}$	$q^{1/2} \Omega \Sigma_{\text{tot}}^{-1/2} \Sigma_{\text{SFR}}^{0.36} T^{1/2}$	$q^{-1} \Omega^{-1} \Sigma_{\text{SFR}}^{1/3} T^{1/3}$
Alt2b	$\Sigma_{\text{tot}}^{-1/2} \Sigma_{\text{SFR}}^{0.69} T^{5/6}$	$q^{1/2} \Omega^{1/2} \Sigma_{\text{tot}}^{-1/2} \Sigma_{\text{SFR}}^{0.52} T^{2/3}$	$q^{1/2} \Omega \Sigma_{\text{tot}}^{1/2} \Sigma_{\text{SFR}}^{0.024} T^{-1/3}$	$q^{-1} \Omega^{-1} \Sigma_{\text{SFR}}^{1/3} T^{1/3}$

6.3. Relations between observables

An important caveat is that the observables $q(r)$, $\Omega(r)$, $\Sigma(r)$, $\Sigma_{\text{SFR}}(r)$, $\Sigma_{\star}(r)$ and $T(r)$ are not mutually statistically independent. For example, the SFR and gas surface densities are typically related by the Kennicutt-Schmidt (KS) law,

$$\Sigma_{\text{SFR}} \propto \Sigma^N, \quad (38)$$

with $N \approx 1.4$ (Kennicutt & Evans 2012). As this relation is rather tight and universal, we have used the KS law to replace Σ by $\Sigma_{\text{SFR}}^{1/N}$ in Tables 5 and 6, eliminating the explicit dependence on Σ . We focus on Tables 5 and 6 in the discussion below.

Other correlations between our observables have also been measured, like the so-called spatially resolved star-forming main sequence relating Σ_{SFR} and Σ_{\star} (e.g. Cano-Díaz et al. 2016; Baker et al. 2022). However, this relation shows quite a lot of scatter. Moreover, the power law exponent, $\partial \ln \Sigma_{\star} / \partial \ln \Sigma_{\text{SFR}}$, is not well-constrained, and may be sensitive to resolution (Hani et al. 2020). For this reason, we treat $\Sigma_{\text{tot}} \approx \Sigma_{\star}$ and Σ_{SFR} as mutually independent quantities.

6.4. Consistency of models across regimes

In Model S (SN-driven model), the exponents in Tables 5 and 6 are remarkably consistent when transitioning between the four different physical regimes. Thus, the results for Model S are fairly insensitive to variations in the Mach number and the ratio of the eddy turnover and renovation times. By contrast, in Model Alt2 (hybrid model) the rms turbulent velocity u has very different power law exponents for the two limiting cases ($\mathcal{M} \ll A$ and $\mathcal{M} \gg A$). This implies a sharp transition in the transonic regime, which seems unlikely from a physical standpoint, lending support to the claim that Model S is the most realistic among the models.

6.5. Comparison with observations

We now compare our results with previously published observations, continuing to focus on Tables 5 and 6, which take into account the KS law, i.e. the empirical relation between Σ and Σ_{SFR} (equation 38).

6.5.1. Turbulent velocity

As seen in Table 5, Model S predicts that the rms turbulent velocity u depends very weakly on Σ_{SFR} and depends weakly on Σ_{tot} and T . One might then expect the variation in the velocity dispersion within a galaxy or between galaxies to be weak. This is borne out in the data. Based on second moment maps of THINGS galaxies (Walter et al. 2008), Leroy et al. (2008) find the 1D velocity dispersion for THINGS galaxies to be $11 \pm 3 \text{ km s}^{-1}$. The gas velocity dispersion within a given galaxy is also fairly constant (e.g. Mogotsi et al. 2016; Chemin et al. 2016). Thus, the predicted weak dependence of u on Σ_{tot} , Σ_{SFR} and T is qualitatively consistent with observations at low redshift.

From Table 5, Model Alt1 predicts u to be independent of the other observables except T , where the $T^{1/2}$ dependence is stronger than for Model S. By contrast, Model Alt2 predicts a strong dependence on the various observables as well as different signs of the exponents for the subsonic and supersonic cases, and thus disagrees with observations.

6.5.2. Relationship between field strength and Σ_{SFR}

It has been observed in many galaxies that the total magnetic field strength correlates with Σ_{SFR} , and many authors have obtained values for j in the relation $B \propto \Sigma_{\text{SFR}}^j$. Niklas & Beck (1997) find $j = 0.34 \pm 0.08$, assuming energy equipartition between magnetic field and cosmic rays. Chyży (2008) finds a tight correlation looking at the spatial variation of B and Σ_{SFR} in the Virgo Cluster spiral galaxy NGC 4254, and obtains $j = 0.18 \pm 0.01$. They also find a tight correlation between the random component (calculated from the unpolarized emission) and Σ_{SFR} , with a power law exponent of 0.26 ± 0.01 . Chyży et al. (2011) find $j = 0.30 \pm 0.04$ for dwarf irregular galaxies. Heesen et al. (2014) infer $j = 0.30 \pm 0.02$ for 17 THINGS galaxies. Van Eck et al. (2015) find $j = 0.19 \pm 0.03$, using results that assume energy equipartition. Wang & Lilly (2022) interpret Heesen et al. (2014) and other observations and assume energy equipartition to obtain $j = 0.15 \pm 0.06$. They show how an exponential profile for $\Sigma_{\text{SFR}}(r)$ – seen in

many disk galaxies – can be explained by their model as long as $0.1 \lesssim j \lesssim 0.2$.

For the galaxy NGC 6946, [Tabatabaei et al. \(2013\)](#) obtain $j = 0.14 \pm 0.01$, and, if B is replaced by the turbulent component (calculated from the unpolarized emission), they obtain an equally strong correlation with a slightly different exponent of 0.16 ± 0.01 . [Vollmer et al. \(2020\)](#) obtain j values between 0.03 and 0.92, with a lot of scatter and a best fit value of either 0.13 ± 0.09 or 0.44, depending on the statistical technique adopted. There has also been a flurry of very recent work. [Heesen et al. \(2023\)](#) find $j = 0.182 \pm 0.004$, but with considerable scatter, or $j = 0.22$ when they use the mean values of each of the 12 galaxies considered. However, when they account for cosmic-ray transport, they infer a value of $j = 0.284 \pm 0.006$ instead of 0.182 ± 0.004 . These authors also report that B is found to be more tightly correlated with the gas surface density $\Sigma = \Sigma_{\text{HI}} + \Sigma_{\text{H}_2}$ than with Σ_{SFR} . [Tabatabaei et al. \(2022\)](#) study the galaxy M33 and find bi-modal behaviour. For the high-SFR regime they obtain $j = 0.25\text{--}0.26$ and for the low-SFR regime they obtain $j = 0.10\text{--}0.12$. [Basu et al. \(2017\)](#) obtains $j = 0.35 \pm 0.03$ for the dwarf irregular galaxy IC 10. Finally, [Manna & Roy \(2023\)](#) obtain $j = 0.31 \pm 0.06$ for a sample of seven galaxies, using the equipartition assumption.

In the present work we have derived expressions for b_{iso} , b_{ani} and \bar{B} , and scaling relations are presented in Table 6. Observers generally infer that the isotropic random component of the magnetic field dominates in most galaxies. Moreover, when a mean component is modeled from the observations, this component is usually determined to be quite weak, suggesting that most of the polarized emission is not due to the mean field, but to an anisotropic small-scale component ([Beck et al. 2019](#)). At face value, this would imply that, typically, $b_{\text{iso}} > b_{\text{ani}} > \bar{B}$. However, the mean field may often be underestimated if, as seems likely, it contains significant power at scales that cannot be resolved.

Examining the scaling relations for b_{iso} , b_{ani} and \bar{B} in Table 6 for Model S, we see that they are related to Σ_{SFR} by power laws with exponents in the ranges 0.34–0.39, 0.21–0.29 and 0.09–0.10, respectively. Thus, if b_{iso} is the dominant field component, a suitable weighted average might give $j \sim 0.30$, whereas if \bar{B} is the dominant component, we might expect $j \sim 0.15$. While a detailed comparison between theory and observation is clearly not possible here, the theoretical and empirical estimates for j agree rather well. Furthermore, the prediction of our model that j is higher for the isotropic random component than for the mean component aligns with the findings of [Chyży \(2008\)](#) and [Tabatabaei et al. \(2013\)](#) (though the latter work finds only a marginal difference), as well as with those of [Tabatabaei et al. \(2022\)](#) if the mean field is relatively stronger in the low-SFR regions.

On the other hand, Model Alt1 predicts $j = 0.36$, which is reasonably consistent with observations, but Model Alt2 predicts an exponent 0.69 for b_{iso} , 0.52 for b_{ani} and a range 0.02–0.36 for \bar{B} , which are too high to explain observations.

These results are summarized in the left panel of Figure 2, where it can be seen that the range predicted by Model S corresponds reasonably well to the range spanned by the data. Keep in mind that in our model j would be a weighted average of the j -values for b_{iso} , b_{ani} and \bar{B} , so the observed values of j would be expected to lie somewhere between the highest and lowest predictions. Taking our Model S at face value, the upper cluster of points between 0.25 and 0.35 is just what might be expected if b_{iso} dominates but b_{ani} and/or \bar{B} are significant, whereas the lower cluster of points between about 0.1 and 0.2 could arise if the mean magnetic field is particularly strong.

A theoretical model by [Schleicher & Beck \(2013\)](#) (see also [Schleicher & Beck 2016](#)) predicts $B \propto \Sigma_{\text{SFR}}^{1/3}$, whereas the model by [Schober et al. \(2023\)](#) (see also [Schober et al. 2016](#)) predicts $B \propto \Sigma_{\text{SFR}}^{1/3} \Sigma^{1/6}$, which gives $B \propto \Sigma_{\text{SFR}}^{0.45}$ if $\Sigma_{\text{SFR}} \propto \Sigma^{1.4}$ is assumed. Those models have similarities with one another. They are also somewhat similar to Model Alt2a of the present work, but their prescriptions for the gas scale height are different from ours.

6.5.3. Relationship between field strength and density

[Manna & Roy \(2023\)](#) obtain $B \propto \rho^{0.40 \pm 0.09}$ for a sample of seven galaxies. Using equations (10), (12), (25) and (23), we find that b_{iso} is almost independent of ρ for Models Sa and Sc, but for Models Sb and Sd we obtain a power law exponent of 1/2 since u cancels out in equation (10) with B_{eq} given by equation (12). For transonic turbulence, we would therefore expect a positive exponent somewhere in between 0 and 1/2, so Model S is broadly consistent with observations. For Model Alt1, $b_{\text{iso}} \propto \rho^{1/2}$ since u is independent of ρ . For Model Alt2a, $l_{\text{SN}} \propto h$, which is independent of ρ , so $b_{\text{iso}} \propto \rho^{1/2}$, while for Model Alt2b, u cancels so that again $b_{\text{iso}} \propto \rho^{1/2}$. Thus, predictions of Models S, Alt1 and Alt2 all broadly agree with the empirical relation.

6.5.4. Relationship between field alignment and Σ_{SFR}

In the study of NGC 4254 mentioned above, [Chyży \(2008\)](#) also found that the ratio of the strength of the magnetic field inferred from polarized emission (comprising mean and anisotropic turbulent components) to that inferred from total emission is negatively correlated with Σ_{SFR} , i.e. $B_{\text{pol}}/B \propto \Sigma_{\text{SFR}}^{-m}$, with $m = 0.32 \pm 0.01$. More recently, [Vollmer et al. \(2020\)](#) measured the same relation, but using data from several galaxies. They find a tight correlation, with $m = 0.22$ or 0.24, depending on the fitting method.

To make a comparison with the model, let us first assume that the polarized emission is dominated by b_{ani} and the total emission by b_{iso} and consider the ratio $b_{\text{ani}}/b_{\text{iso}}$ using results

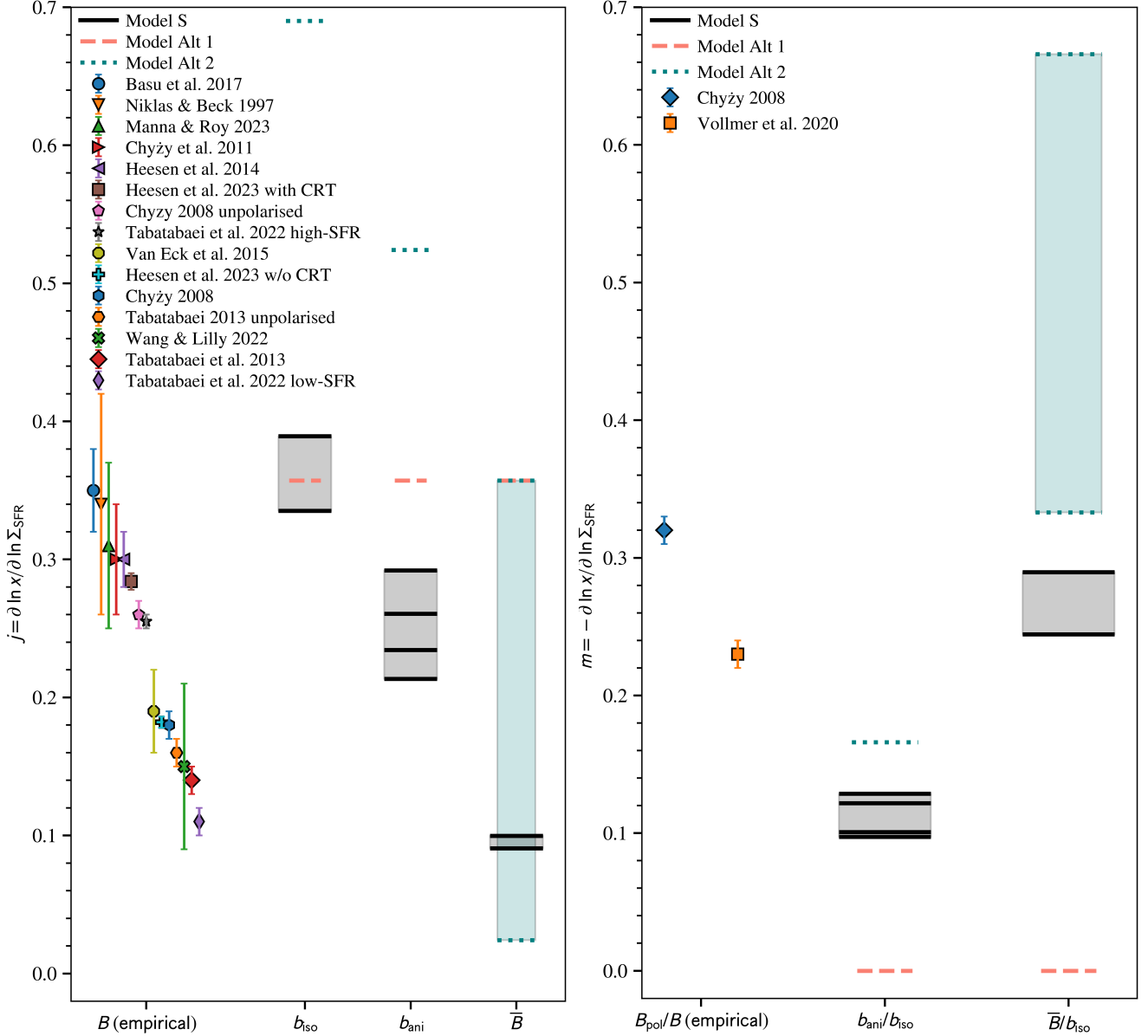


Figure 2. The left panel compares the quantity $j = \partial \ln B / \partial \ln \Sigma_{\text{SFR}}$ inferred from observations (symbols) with the values of $\partial \ln b_{\text{iso}} / \partial \ln \Sigma_{\text{SFR}}$, $\partial \ln b_{\text{ani}} / \partial \ln \Sigma_{\text{SFR}}$, and $\partial \ln \bar{B} / \partial \ln \Sigma_{\text{SFR}}$ obtained from Models S, Alt1, and Alt2 (horizontal lines). The range spanned by the data is quite consistent with the predictions of the fiducial model, Model S. In the right panel, data points show the scaling relation exponent $m = -\partial \ln (B_{\text{pol}}/B) / \partial \ln \Sigma_{\text{SFR}}$ inferred from observations. Horizontal lines and ranges show the predictions of our models when B_{pol} is assumed to be dominated by b_{ani} or \bar{B} , and B by b_{iso} . Predictions of the fiducial model, Model S, with parameters chosen such that $\bar{B} \gg b_{\text{ani}}$, are quite consistent with the data.

from Table 6. For Model S, we obtain $m = 0.13, 0.13, 0.11$ and 0.10 , respectively. Therefore, the correct sign of the exponent is reproduced in the model, but its magnitude is lower than the observational values. For Model Alt1, we obtain $m = 0$, which is in disagreement with the observations. For Model Alt2, we obtain $m = 0.17$, which is quite close to the observational values.

However, if \bar{B} actually dominates the polarized emission, then we should use \bar{B}/b_{iso} instead of $b_{\text{ani}}/b_{\text{iso}}$. In this case,

Model S predicts values of m in the range 0.25 - 0.29 , which is very close to the observed values. On the other hand, Model Alt1 again predicts $m = 0$, while Model Alt2a and Alt2b predict $m = 0.33$ and $m = 0.67$, respectively. These results are summarized in the right panel of Figure 2, which illustrates that Model S is quite consistent with the data only if $B_{\text{pol}}/B \sim \bar{B}/b_{\text{iso}}$, which implies $b_{\text{iso}} > \bar{B} > b_{\text{ani}}$. This ordering of b_{iso} , \bar{B} and b_{ani} is possible in our model, given the freedom in the parameter choices. However, if this in-

terpretation is correct, it would suggest that the mean field may often be underestimated when interpreting radio observations of nearby galaxies, since such studies typically find that $b_{\text{ani}} > \bar{B}$. We note, however that different kinds of averages are used in theory and observations, which complicates their comparison (Beck et al. 2019).

6.5.5. Other dependencies of magnetic field properties

Van Eck et al. (2015) explored the dependencies of the total field strength, mean field strength and mean field pitch angle, as obtained from observations (supplemented by the usual assumption of equipartition between magnetic and cosmic ray energies). The observables they explored as independent quantities were the H I surface density Σ_I , molecular gas surface density Σ_2 , their sum $\Sigma_I + \Sigma_2$, Σ_{SFR} , Ω , $q\Omega$ and $q\Omega^2$. They also looked for statistical relationships between B , \bar{B} and p_B .⁸ Of these 24 pairs of variables, 10 were found to exhibit correlations. We now look at each of these and compare them with the findings in Table 6.

As mentioned in Section 6.5.2, Van Eck et al. (2015) obtained $B \propto \Sigma_{\text{SFR}}^{0.19 \pm 0.03}$, with B the strength of the total field. They also obtained $B \propto \Sigma_2^{0.21 \pm 0.04}$ and $B \propto (\Sigma_I + \Sigma_2)^{0.24 \pm 0.07}$. These latter two can be interpreted as a confirmation of Schmidt/KS laws, given the relationship found between B and Σ_{SFR} . However, the value of N implied is slightly lower than 1.4.

The fourth and fifth correlations obtained were between B and $q\Omega$ (power law not given) and $B \propto (q\Omega^2)^{0.14 \pm 0.04}$. If the total field strength were dominated by b_{iso} , then Table 6 would predict no dependence, i.e. no correlation. If dominated by \bar{B} , then Table 6 would predict a power of 0.5. Thus, the observed value of 0.14 ± 0.04 is intermediate between these values, suggesting that the mean field tends to be significant, but not dominant. The dependence of b_{ani} on q and Ω (but not explicitly on $q\Omega^2$ in the model) likely also plays a role.

The sixth, seventh and eighth correlations found by Van Eck et al. (2015) were $\tan p_B \propto \Sigma_2^{-0.10 \pm 0.08}$, $\tan p_B \propto (\Sigma_I + \Sigma_2)^{-0.25 \pm 0.13}$ and $\tan p_B \propto \Sigma_{\text{SFR}}^{-0.15 \pm 0.09}$. These are approximately related by the Schmidt/KS law, as expected, so let us consider only the last relation. The exponent is similar to that predicted for Model S in Table 6, where we obtain $-(0.13-0.29)$, depending on the exact regime ($\tau_e/\tau_r < 1$ or > 1 , and $\mathcal{M} \ll 1$ or $\gg 1$). On the other hand, Model Alt1 predicts no dependence and Model Alt2 predicts an exponent equal to positive 1/3, so Model S is compatible with observations, but Models Alt1 and Alt2 are not.

⁸ What Van Eck et al. (2015) interpret as \bar{B} may in some cases contain a contribution from anisotropic random field (b_{ani} in our model; c. f. Beck et al. 2019). For the purpose of comparing our model results with the findings of Van Eck et al. (2015), we ignore this complication and directly compare our model with their final results; a re-analysis of the data is left for future work.

6.5.6. Relation between mean and total field strengths

The ninth correlation found by Van Eck et al. (2015) can be described by the power law $\bar{B} \propto B^{0.76 \pm 0.23}$. Given that the powers of the observables generally have the same sign in Model S for b_{iso} , b_{ani} and \bar{B} (Table 6), one would expect the scaling between \bar{B} and B to have a positive exponent, consistent with the above observation. The exception is the power of the gas temperature T . However, T does not usually vary as much as some of the other parameters in galaxies, where warm gas is the dominant volume-filling phase of the ISM, and retains a temperature of order 10^4 K. In addition, one might expect the power to be < 1 , as observed, since the exponents in the scaling relation for \bar{B} are generally smaller than those in the scaling relations for b_{iso} and b_{ani} , but not very small because \bar{B} itself contributes significantly to B . Therefore, Model S again gives results that are broadly consistent with observations. For Models Alt1 and Alt2, the exponents of Σ_{tot} tend to change sign when going from \bar{B} to b_{iso} , so the correlation between \bar{B} and B seems harder to explain using these alternative models.

6.5.7. Relation between mean field strength and pitch angle

The final correlation detected by Van Eck et al. (2015) – between \bar{B} and p_B – was the most statistically significant. Though the power law fit was not provided, the magnitude of p_B was found to decrease as \bar{B} increases. This trend was confirmed by Beck et al. (2019), using updated data. Given this negative correlation, one might expect the exponents in the scaling relations for \bar{B} and p_B to generally have opposite signs. The powers of q , Ω and Σ_{SFR} have opposite signs in the expressions for \bar{B} and $\tan p_B$ of Model S, while those of Σ_{tot} have the same sign, and those of T are the same in three of four cases. Thus, more work is needed to understand this empirical relation using dynamo models.

6.5.8. Cases where no empirical scaling relation was found

For the remaining 14 relationships explored by Van Eck et al. (2015), no statistically significant correlation was found. Can these null results be explained by Model S? One such result was that \bar{B} was not found to depend significantly on any of Σ_{SFR} , Σ_I , Σ_2 , $\Sigma_I + \Sigma_2$, Ω , $q\Omega$ or $q\Omega^2$. Model S predicts only a weak dependence on most of these, but one would expect to find $\bar{B} \propto (q\Omega^2)^{1/2}$ in all of the models. Moreover, $\tan p_B$ would be expected to scale as $(q\Omega)^{-1}$ in all the models, whereas no such correlation was found by Van Eck et al. (2015). More work is needed to understand why models and data seem to disagree about this particular aspect.

6.5.9. Arm-interarm contrast of random and mean fields

Model S predicts (Table 6) that for lower Σ_{SFR} or Σ_{tot} , the ratio \bar{B}/b_{iso} should increase. This suggests that the field should be coherent on larger scales in the interarm regions, where Σ_{SFR} and Σ_{tot} are smaller than in the arms.

When the arm-interarm contrast of \bar{B}/b_{iso} can be estimated from observations this ratio is inferred – particularly for the galaxy NGC 6946 where the data is of good quality – to be higher within the interarm regions (Beck & Hoernes 1996), consistent with our model predictions. On the other hand, Model Alt1 predicts that \bar{B}/b_{iso} should decrease with Σ_{tot} but not depend on Σ_{SFR} and Model Alt2 predicts that \bar{B}/b_{iso} should decrease with Σ_{SFR} but not depend on (increase with) Σ_{\star} if $\mathcal{M} \ll A$ ($\gg A$), so again, Models Alt1 and Alt2 do not agree with the observations as well as our SN-driven turbulence model, Model S.

6.6. Comparison with simulations

Elstner & Gressel (2012) is the only work of which we are aware that obtains such scaling relations from direct numerical simulations (Gressel et al. 2008a, 2011). These authors employ simulations of SN-driven turbulence to study dynamo action in a small section of a galaxy. They provide scaling relations for a few quantities, based on nine simulations. In seven of their runs, the final magnetic field energy is of order the turbulent energy, but in the other two the simulation ends when $B \ll B_{\text{eq}}$, so those runs are less relevant. They also find that both vertical outflows and diamagnetic pumping are important, but these effects have been neglected in deriving the scaling relations found in the present work.

Given the differences between their model and ours, it is perhaps most useful to compare results for the turbulent diffusivity η because this quantity is not expected to be sensitive to details such as the dynamo saturation mechanism (Brandenburg & Subramanian 2005). Elstner & Gressel (2012) find $\eta \propto \sigma^{0.4} n^{0.4} \Omega^{-0.55}$, where σ is the SFR density in dimensions of $[\text{T}]^{-1} [\text{L}]^{-2}$, and, as above, n and Ω are the number density of gas and the rotation angular speed, respectively. The value of σ is determined from their input SN rate assuming a constant initial mass function, so we can replace σ with Σ_{SFR} , resulting in $\eta \propto \Sigma_{\text{SFR}}^{0.4} n^{0.4} \Omega^{-0.55}$.

To compare this result with our models, we derive scaling relations using equation (18), the scaling relations of Table 3, and equation (30), and assume $\rho/n = \text{const}$. We use Table 3 rather than Table 5 because the overall SN rate density is varied as a parameter in the Elstner & Gressel (2012) simulations.⁹ Neglecting the temperature dependence, Models Sa-d respectively give $\eta \propto \Sigma_{\text{SFR}}^{1/3} n^{-0.9} \Sigma_{\text{tot}}^{0.4}$, $\eta \propto \Sigma_{\text{SFR}}^{0.2} n^{-0.7} \Sigma_{\text{tot}}^{0.2}$, $\eta \propto \Sigma_{\text{SFR}}^{-1/3} n^{0.1} \Sigma_{\text{tot}}^{-0.3}$ and $\eta \propto n^{-0.1} \Sigma_{\text{tot}}^{-0.4}$ (where in the last relation we have neglected the very weak dependence on Σ_{SFR}). Models Alt1, Alt2a and Alt2b give $\eta \propto \Sigma_{\text{tot}}^{-1}$, $\eta \propto \Sigma_{\text{SFR}}^{1/3} \Sigma_{\text{tot}}^{-2}$ and $\eta \propto \Sigma_{\text{SFR}}^{-1} \Sigma_{\text{tot}}^2$, respectively. Given that Ω depends on the

gravitational potential, Ω and Σ_{tot} are not completely independent from one another. Thus, the absence of Ω in our scaling relations for η does not necessarily imply disagreement with Elstner & Gressel (2012). For this reason, let us focus on Σ_{SFR} and n . In Models Sa, Sb and Alt2a, we find Σ_{SFR} exponents of 1/3, 0.2 and 1/3, respectively, which are close to the value of 0.4 obtained by Elstner & Gressel (2012). In the other models, the agreement is poorer, with exponents $-1/3$, ≈ 0 , 0 and -1 , for Models Sc, Sd, Alt1 and Alt2b, respectively. Now turning to the dependence on n , we obtain a positive exponent only for Model Sc (0.1), whereas other models give exponents ranging from -0.9 to 0, which is in disagreement with the value of 0.4 obtained by Elstner & Gressel (2012). We can conclude that the level of agreement between our predicted scaling relation for η and that found by Elstner & Gressel (2012) is rather poor. However, the dependence on Σ_{SFR} agrees quite well in Model S whenever $\tau_e < \tau_r$ and in Model Alt2a, where $\mathcal{M} \ll A$ (although Gressel et al. 2008b report mildly supersonic turbulence for the simulations of that paper, so Alt2b is probably more relevant than Alt2a, but there the model predicts a dependence on Σ_{SFR} different from that seen in the simulations).

In addition, Gressel et al. (2008a) report that the ratio of the strength of the mean field to that of the random field is related to the SN rate (SFR density) as $\bar{B}/b \propto \Sigma_{\text{SFR}}^{-0.38 \pm 0.01}$, while for similar simulations by Bendre et al. (2015) the authors report $\bar{B}/b \propto \Sigma_{\text{SFR}}^{-0.30 \pm 0.07}$. Generally, we expect $b_{\text{iso}} > b_{\text{ani}}$ (Beck et al. 2019), so we focus on the ratio \bar{B}/b_{iso} , using Table 4. For Model Alt1 we find no dependence of \bar{B}/b_{iso} on Σ_{SFR} . For Models Alt2a and Alt2b we find $\bar{B}/b_{\text{iso}} \propto \Sigma_{\text{SFR}}^{-1/3}$ and $\bar{B}/b_{\text{iso}} \propto \Sigma_{\text{SFR}}^{-2/3}$, respectively. For Models Sa and Sc, we find $\bar{B}/b_{\text{iso}} \propto \Sigma_{\text{SFR}}^{-1/3}$, and for Models Sb and Sd we find $\bar{B}/b_{\text{iso}} \propto \Sigma_{\text{SFR}}^{0.37}$. Thus, for Models Alt2a, Sa and Sc (all of which have $\mathcal{M} \ll A$) the agreement is good, for Model Alt2b the agreement is fair, and for Models Sb and Sd the agreement is poor. Differences may be partly attributable to the different physical assumptions between our models and those of Elstner & Gressel (2012). However, there is another important caveat, namely that the separation of the magnetic field into random and mean components may be sensitive to the method of averaging. The mean-field dynamo theory on which our models are founded assumes ensemble averaging, while Gressel et al. (2008a) use horizontal averaging.

6.7. Scaling relation proportionality coefficients

Thus far we have focused on the scaling relation exponents. We now make an order-of-magnitude estimate of the proportionality coefficients in the magnetic field strength vs. Σ_{SFR} relations. This is important for checking that the magnitude of the magnetic field strengths predicted by the model roughly agree with observational and theoretical expectations. We must first fix the values of the other observables; this is done

⁹In their simulations, the SN rate density is higher where the gas density is higher, but the overall normalization of the SN rate surface density is set by hand, independently of the gas profile, and varied from one simulation to another to isolate the effects of this one parameter (Bendre et al. 2015).

Table 7. Typical numerical coefficients \tilde{B}_i for scaling relations of the form $B_i = \tilde{B}_i (\Sigma_{\text{SFR}}/\tilde{\Sigma})^j$, where $\tilde{\Sigma} = 10^{-3} \text{ M}_\odot \text{ yr}^{-1} \text{ kpc}^{-2}$, for two different estimates of the numerical coefficient in the Kennicutt-Schmidt law relating Σ_{SFR} and Σ (see Section 6.7 for details). Fitting data for the total magnetic field strength in multiple galaxies (estimated assuming energy equipartition with cosmic rays), Heesen et al. (2023) obtain \tilde{B} in the range 4.7–7.4 μG . Our model coefficients are generally of the same order of magnitude as theirs. All field strengths are in μG and the KS relation coefficient is in cgs units.

KS coef.	Model S			Model Alt1			Model Alt2		
	b_{iso}	b_{ani}	\tilde{B}	b_{iso}	b_{ani}	\tilde{B}	b_{iso}	b_{ani}	\tilde{B}
10^{-15}	10	2	1	8	3	3	12	4	3
10^{-16}	44	16	2	20	7	6	28	10	6

by choosing a typical value based on data for the galaxies M31, M33, M51 and NGC 6946, which are the galaxies studied in Paper II (in preparation). We choose $\Omega = 20 \text{ km s}^{-1} \text{ kpc}^{-1}$, $\Sigma = 5 \text{ M}_\odot \text{ pc}^{-2}$, and $\Sigma_{\text{tot}} = 175 \text{ M}_\odot \text{ pc}^{-2}$, respectively. In addition we choose $T = 10^4 \text{ K}$ and $q = 1$. Further, the adjustable parameters of the model are chosen to be values that generally produce good agreement with the velocity dispersion and magnetic field data in the preliminary analysis of Paper II: $\zeta = 10$, $\beta = 8$, $C_\alpha = 4$, and $K = 0.3$.

The scaling law can be written as

$$B = \tilde{B} \left(\frac{\Sigma_{\text{SFR}}}{\tilde{\Sigma}} \right)^j, \quad (39)$$

where $\tilde{\Sigma} = 10^{-3} \text{ M}_\odot \text{ yr}^{-1} \text{ kpc}^{-2}$ is a typical value of the SFR surface density and \tilde{B} is the coefficient we want to estimate. To calculate \tilde{B} , we also need a proportionality coefficient for the KS relation $\Sigma_{\text{SFR}} = C \Sigma^N$. Using the data for Σ_{SFR} and Σ used in Paper II, and assuming $N = 1.4$, we obtain $C \approx 10^{-15}$ in cgs units. As an alternative, we estimated the coefficient from Leroy et al. (2008), who found that the star formation efficiency is, on average, $\sim 3 \times 10^{-10} \text{ yr}^{-1}$, for $\Sigma \approx 5\text{--}10 \text{ M}_\odot \text{ pc}^{-2}$. For $N = 1.4$, this leads to $C \approx 10^{-16}$ in cgs units. Then, with these values, we obtain the values in Table 6.7. These rough estimates are consistent, at the order-of-magnitude level, with those of Heesen et al. (2023), who estimate a range 4.7–7.4 μG for \tilde{B} . Moreover, we generally find $b_{\text{iso}} > b_{\text{ani}} > \tilde{B}$, which is consistent with the usual ordering inferred by Beck et al. (2019). We note, however, that this ordering can be sensitive to the parameters of our model.

7. SUMMARY AND CONCLUSIONS

We have presented a model for the turbulence parameters and magnetic field properties of disk galaxies that takes as input various observables. The set of algebraic equations comprising the model can be solved semi-analytically using the source code linked in Section 2. Solutions depend

on the galactocentric radius and represent averages over the azimuthal and vertical coordinates. The model rests on the assumption that the system is in a statistically steady state, and any dependence on the cosmological redshift is neglected, so our solutions are applicable to nearby galaxies (though extending the model to include higher redshifts would be an interesting direction). Figure 1 summarizes the structure of the model. A list of the quantities and parameters in the model and the equations for computing them can be found in Table 1.

7.1. Scaling relations

We used the model to derive scaling relations for the gas scale height, key turbulence parameters and magnetic field properties, in terms of the observables. These are relations of the form $X \propto x^a y^b z^c \dots$, where X is a quantity of interest, x , y and z are observable quantities, and a , b and c are constants. Scaling relations are useful for placing priors on missing information in datasets and for providing physical insight, and are ubiquitous in astrophysics. The scaling relations can be derived analytically, but we provide a link to a general numerical tool in Section 2. To reduce the solutions to scaling relations, we focused on certain plausible asymptotic regimes. Most importantly, we assumed that turbulence is driven purely by isolated SNe and that mean (large-scale) vertical and radial gas motions can be neglected. In deriving scaling relations for the mean magnetic field strength, we assumed that the Coriolis number is small and that the dynamo is strong (Section 6), but these assumptions were not necessary for deriving scaling relations for the pitch angle of the mean field.

These scaling relations can be found in Tables 3 and 4. Our fiducial model considers turbulence to be driven by isolated SNRs, as they decelerate to the sound speed and merge with the ISM. Given the lack of consensus about turbulence driving in the ISM, we also considered two simpler prescriptions for calculating the turbulence parameters, as summarized in Table 2.

The predictions in Tables 3 and 4 do not consider possible correlations between the observed quantities on the right side of the scaling relations. Given the well-known empirical relation between Σ_{SFR} and Σ (the Kennicutt-Schmidt law), we used $\Sigma_{\text{SFR}} \propto \Sigma^N$ with $N = 1.4$ to eliminate the dependence on Σ , and the results are presented in Tables 5 and 6.

The theoretical scaling relations in Tables 5 and 6 were then compared with empirical scaling relations in the literature (Section 6.5). The level of agreement between the model predictions and observations is remarkably good for our fiducial model, Model S, given the various theoretical and observational uncertainties. The level of agreement is generally poorer for the alternative turbulence prescriptions we tried (Models Alt1 and Alt2). This can be taken as further evidence that turbulence driving in nearby galaxies is dom-

inated by SN feedback. It also suggests that assuming that turbulence is driven at the disk scale height can lead to incorrect results, and points to a need for modeling turbulence driving in more detail, taking into account the dynamics of SNRs.

7.2. Limitations and future work

Our model should be thought of as an adaptable tool for understanding galactic magnetic fields rather than a fixed set of formulae. This tool could be extended by including additional physical effects. Outflows and SBs (which tend to cause outflows) are already included in the most general version of our model, summarized in Appendix A, but including these effects introduces extra parameters that are challenging to constrain. SBs may be unlikely to dominate turbulence driving because they tend to blow out of the disk, which limits the amount of energy they transfer to the ISM (Boomsma et al. 2008; Chamandy & Shukurov 2020). Likewise, rough estimates suggest that mean outflow speeds may often be too small to strongly affect mean-field dynamo action (Chamandy et al. 2016). However, such findings are preliminary and more work is needed on the roles of SBs and outflows in turbulence driving and magnetic field evolution. Furthermore, our model does not include radial inflow (e.g. Schmidt et al. 2016; Trapp et al. 2022), which may affect the mean-field dynamo (Moss et al. 2000) and play a role in driving interstellar turbulence, though primarily at high redshift (Krumholz et al. 2018).

On the MHD side, we have not included the turbulent tangling of the mean field to produce random field, nor additional effects – still not very well-understood – involving the influence of the random field on the mean-field dynamo (e.g. Chamandy & Singh 2018; Gopalakrishnan & Subramanian 2023). Furthermore, the equations for the turbulence parameters, gas scale height, etc., do not take into account the magnetic field. This is hard to avoid given the lack of current knowledge about such feedback effects, and attempting to include them would make the model more complicated without providing much benefit, given the various uncertainties. Nevertheless, such effects may be important (e.g. Evirgen et al. 2019). In some cases, they can be roughly included in our existing model by choices of parameter values; for example, the effect of the magnetic pressure on the gas scale height can be included heuristically by increasing the value of ζ in equation (32).

Our model does not consider cosmological evolution, but there is scope for extending the model to include high redshift galaxies (Schleicher & Beck 2013; Krumholz et al. 2018; Schober et al. 2023).

There is scope for combining our model with galaxy models that rely on certain magnetic field parameters as input in order to calculate those parameters self-consistently. For example, as mentioned in the introduction, the galaxy model

of Wang & Lilly (2022) depends critically on the exponent in the scaling relation between total magnetic field strength B and SFR surface density Σ_{SFR} , as do theoretical models of the infrared-radio correlation (e.g. Schleicher & Beck 2013). In our model, there is — in the strict sense, at least — no scaling relation between total field strength B and Σ_{SFR} because $B = (b_{\text{iso}}^2 + b_{\text{ani}}^2 + \bar{B}^2)^{1/2}$, with each component having its own separate scaling relation (for b_{ani} and \bar{B} , that too only in certain plausible asymptotic limits). However, the exponents in each of these relations lie in the range 0.1–0.4 for our fiducial model, Model S (Table 6), and this range is broadly consistent with the values inferred from observations (Section 6.5.2 and the left panel of Fig. 2). Thus, our model can be seen as a possible refinement to models that assume that B simply scales with B_{eq} (defined in equation 12) without other scalings. Even if $B/B_{\text{eq}} = \text{const}$ is assumed, one still needs a relation between the rms turbulent speed u and Σ_{SFR} . Our fiducial model, Model S, predicts a very weak dependence of u on Σ_{SFR} , with power-law exponent in the range -0.03 to -0.02 (Table 5). Here again, our model, which includes a detailed model of turbulence driving by SNe, can be seen as a possible refinement to other approaches.

Modeling scaling relations can be complicated by correlations between the observables. While we used the KS relation to remove Σ as an independent variable, we made no attempt to incorporate the resolved star-forming main sequence relation between Σ_{\star} and Σ_{SFR} , for instance. If this could be used to eliminate Σ_{\star} , it would affect the Σ_{SFR} -dependence of the scaling relations derived. Nor did we attempt to relate the angular rotation speed Ω with the disk surface density Σ_{tot} , for example, though they are not completely independent. Another caveat is that parameters like ζ may vary somewhat between galaxies, which would introduce scatter.

Observationally derived scaling relations for magnetic fields are now plentiful and will improve as new instruments like the Square Kilometre Array become available. This increases the urgency of studying such scaling relations theoretically, and in our view various complementary approaches can be utilized. For instance, one could make use of a population synthesis model that solves for the magnetic fields of galaxies using the output of a semi-analytic model of galaxy formation as input (Rodrigues et al. 2015, 2019). Second, one could run several local ISM simulations to explore the parameter space, building on the work begun by Elstner & Gressel (2012). Third, one could explore scaling relations using cosmological zoom MHD simulations (e.g. Pakmor et al. 2024). Given the heterogeneous nature of galaxies, such a multi-pronged statistical approach may be very useful for learning about galactic magnetic fields and the various processes that shape them.

ACKNOWLEDGEMENTS

We are indebted to Anvar Shukurov for providing detailed comments on the manuscript and for ongoing discussions about galactic magnetism and interstellar turbulence. We are grateful to the referee for a constructive report that led to improvements to the presentation. We also thank Rainer Beck for insightful comments on both an early and a recent version

of the manuscript, and Jennifer Schober and Luiz Felipe S. Rodrigues for discussions.

DATA AVAILABILITY

There is no additional data to report.

REFERENCES

- Bacchini, C., Fraternali, F., Iorio, G., et al. 2020, *A&A*, 641, A70
- Baker, W. M., Maiolino, R., Bluck, A. F. L., et al. 2022, *MNRAS*, 510, 3622
- Basu, A., Roychowdhury, S., Heesen, V., et al. 2017, *MNRAS*, 471, 337
- Beck, R., Brandenburg, A., Moss, D., Shukurov, A., & Sokoloff, D. 1996, *ARA&A*, 34, 155
- Beck, R., Chamandy, L., Elson, E., & Blackman, E. G. 2019, *Galaxies*, 8, 4
- Beck, R., & Hoernes, P. 1996, *Nature*, 379, 47
- Beck, R., Poezd, A. D., Shukurov, A., & Sokoloff, D. D. 1994, *A&A*, 289, 94
- Bendre, A., Gressel, O., & Elstner, D. 2015, *Astronomische Nachrichten*, 336, 991
- Blackman, E. G., & Field, G. B. 2002, *Physical Review Letters*, 89, 265007
- Boomsma, R., Oosterloo, T. A., Fraternali, F., van der Hulst, J. M., & Sancisi, R. 2008, *A&A*, 490, 555
- Brandenburg, A., & Subramanian, K. 2005, *PhR*, 417, 1
- Burkhart, B. 2021, *PASP*, 133, 102001
- Cano-Díaz, M., Sánchez, S. F., Zibetti, S., et al. 2016, *ApJ*, 821, L26
- Chamandy, L. 2016, *MNRAS*, 462, 4402
- Chamandy, L., & Shukurov, A. 2020, *Galaxies*, 8, 56
- Chamandy, L., Shukurov, A., Subramanian, K., & Stoker, K. 2014, *MNRAS*, 443, 1867
- Chamandy, L., Shukurov, A., & Taylor, A. R. 2016, *ApJ*, 833, 43
- Chamandy, L., & Singh, N. K. 2018, *MNRAS*, 481, 1300
- Chemin, L., Huré, J.-M., Soubiran, C., et al. 2016, *A&A*, 588, A48
- Chyży, K. T. 2008, *A&A*, 482, 755
- Chyży, K. T., Weźgowiec, M., Beck, R., & Bomans, D. J. 2011, *A&A*, 529, A94
- Elmegreen, B. G. 1989, *ApJ*, 338, 178
- Elstner, D., & Gressel, O. 2012, in *Magnetic Fields in the Universe III - From Laboratory and Stars to Primordial Structures*, 151
- Evirgen, C. C., Gent, F. A., Shukurov, A., Fletcher, A., & Bushby, P. J. 2019, *MNRAS*, 488, 5065
- Federrath, C., Chabrier, G., Schober, J., et al. 2011, *PhRvL*, 107, 114504
- Fletcher, A., Beck, R., Shukurov, A., Berkhuijsen, E. M., & Horellou, C. 2011, *MNRAS*, 412, 2396
- Forbes, J., Krumholz, M., & Burkert, A. 2012, *ApJ*, 754, 48
- Gent, F. A., Mac Low, M.-M., & Korpi-Lagg, M. J. 2024, *ApJ*, 961, 7
- Gent, F. A., Mac Low, M.-M., Korpi-Lagg, M. J., & Singh, N. K. 2023, *ApJ*, 943, 176
- Gopalakrishnan, K., & Subramanian, K. 2023, *ApJ*, 943, 66
- Gressel, O., Elstner, D., & Rüdiger, G. 2011, in *Advances in Plasma Astrophysics*, IAU Symp. 274, ed. A. Bonanno, E. de Gouveia Dal Pino, & A. G. Kosovichev, 348–354
- Gressel, O., Elstner, D., Ziegler, U., & Rüdiger, G. 2008a, *A&A*, 486, L35
- Gressel, O., Ziegler, U., Elstner, D., & Rüdiger, G. 2008b, *Astronomische Nachrichten*, 329, 619
- Hani, M. H., Hayward, C. C., Orr, M. E., et al. 2020, *MNRAS*, 493, L87
- Heesen, V., Brinks, E., Leroy, A. K., et al. 2014, *AJ*, 147, 103
- Heesen, V., Klocke, T. L., Brügggen, M., et al. 2023, *A&A*, 669, A8
- Higdon, J. C., & Lingenfelter, R. E. 2005, *ApJ*, 628, 738
- Hollins, J. F., Sarson, G. R., Shukurov, A., Fletcher, A., & Gent, F. A. 2017, *ApJ*, 850, 4
- Kennicutt, R. C., & Evans, N. J. 2012, *ARA&A*, 50, 531
- Kleeorin, N., & Ruzmaikin, A. A. 1982, *Magnetohydrodynamics*, 18, 116
- Klessen, R. S., & Glover, S. C. O. 2016, in *Saas-Fee Advanced Course*, Vol. 43, *Saas-Fee Advanced Course*, ed. Y. Revaz, P. Jablonka, R. Teyssier, & L. Mayer, 85
- Krause, F., & Rädler, K.-H. 1980, *Mean-field magnetohydrodynamics and dynamo theory* (Pergamon Press, Oxford)
- Kroupa, P. 2008, in *Astronomical Society of the Pacific Conference Series*, Vol. 390, *Pathways Through an Eclectic Universe*, ed. J. H. Knapen, T. J. Mahoney, & A. Vazdekis, 3
- Krumholz, M. R., Burkhart, B., Forbes, J. C., & Crocker, R. M. 2018, *MNRAS*, 477, 2716
- Leroy, A. K., Walter, F., Brinks, E., et al. 2008, *AJ*, 136, 2782
- Manna, S., & Roy, S. 2023, *ApJ*, 944, 86
- Mitra, D., Candelaresi, S., Chatterjee, P., Tavakol, R., & Brandenburg, A. 2010, *Astronomische Nachrichten*, 331, 130
- Mogotsi, K. M., de Blok, W. J. G., Caldú-Primo, A., et al. 2016, *AJ*, 151, 15
- Mogotsi, K. M., & Romeo, A. B. 2019, *MNRAS*, 489, 3797
- Monin, A. S., & Yaglom, A. M. 2007, *Statistical Fluid Mechanics: Mechanics of Turbulence*, Vols I and II (Mineola: Dover)

- Moss, D. 1995, *MNRAS*, 275, 191
- Moss, D., Shukurov, A., & Sokoloff, D. 2000, *A&A*, 358, 1142
- Niklas, S., & Beck, R. 1997, *A&A*, 320, 54
- Pakmor, R., Bieri, R., van de Voort, F., et al. 2024, *MNRAS*, 528, 2308
- Phillips, A. 2001, *Geophysical and Astrophysical Fluid Dynamics*, 94, 135
- Pouquet, A., Frisch, U., & Leorat, J. 1976, *Journal of Fluid Mechanics*, 77, 321
- Rädler, K.-H., Kleeorin, N., & Rogachevskii, I. 2003, *Geophysical and Astrophysical Fluid Dynamics*, 97, 249
- Rodrigues, L. F. S., Chamandy, L., Shukurov, A., Baugh, C. M., & Taylor, A. R. 2019, *MNRAS*, 483, 2424
- Rodrigues, L. F. S., Shukurov, A., Fletcher, A., & Baugh, C. M. 2015, *MNRAS*, 450, 3472
- Ruzmaikin, A. A., Shukurov, A. M., & Sokoloff, D. D. 1988, *Magnetic Fields of Galaxies* (Kluwer, Dordrecht)
- Schleicher, D. R. G., & Beck, R. 2013, *A&A*, 556, A142
- . 2016, *A&A*, 593, A77
- Schmidt, T. M., Bigiel, F., Klessen, R. S., & de Blok, W. J. G. 2016, *MNRAS*, 457, 2642
- Schober, J., Sargent, M. T., Klessen, R. S., & Schleicher, D. R. G. 2023, *A&A*, 679, A47
- Schober, J., Schleicher, D. R. G., & Klessen, R. S. 2016, *ApJ*, 827, 109
- Seta, A., & Federrath, C. 2021, *Physical Review Fluids*, 6, 103701
- Shukurov, A. 2004, arXiv e-prints, astro
- Shukurov, A. 2005, in *Lecture Notes in Physics*, Berlin Springer Verlag, Vol. 664, *Cosmic Magnetic Fields*, ed. R. Wielebinski & R. Beck, 113
- Shukurov, A., Sokoloff, D., Subramanian, K., & Brandenburg, A. 2006, *A&A*, 448, L33
- Shukurov, A. M., & Subramanian, K. 2021, *Astrophysical Magnetic Fields: From Galaxies to the Early Universe* (Cambridge: Cambridge University Press), doi:10.1017/9781139046657
- Subramanian, K., & Brandenburg, A. 2006, *ApJ*, 648, L71
- Subramanian, K., & Mestel, L. 1993, *MNRAS*, 265, 649
- Sur, S., Shukurov, A., & Subramanian, K. 2007, *MNRAS*, 377, 874
- Tabatabaei, F. S., Schinnerer, E., Murphy, E. J., et al. 2013, *A&A*, 552, A19
- Tabatabaei, F. S., Cotton, W., Schinnerer, E., et al. 2022, *MNRAS*, 517, 2990
- Trapp, C. W., Kereš, D., Chan, T. K., et al. 2022, *MNRAS*, 509, 4149
- Van Eck, C. L., Brown, J. C., Shukurov, A., & Fletcher, A. 2015, *ApJ*, 799, 35
- Vandenbroucke, B., De Rijcke, S., Schroyen, J., & Jachowicz, N. 2013, *ApJ*, 771, 36
- Vollmer, B., Soida, M., Beck, R., & Powalka, M. 2020, *A&A*, 633, A144
- Walter, F., Brinks, E., de Blok, W. J. G., et al. 2008, *AJ*, 136, 2563
- Wang, E., & Lilly, S. J. 2022, *ApJ*, 927, 217

APPENDIX

A. GENERALIZATIONS OF THE MODEL

Above, we neglected galactic outflows. Applying an expression for the mean outflow speed U_0 derived in [Van Eck et al. \(2015\)](#) (see also [Shukurov et al. 2006](#); [Rodrigues et al. 2015](#)), [Chamandy et al. \(2016\)](#) found outflows to affect negligibly the mean magnetic field properties for the five galaxies for which the data to compute this quantity was available. Even so, outflows may still have important effects, and in Section A.1, we present mean-field dynamo equations for the case $U_0 \neq 0$.

If turbulence driving by SBs is important, the mean magnetic field then also depends on the fraction of SNe that contribute to SBs, f_{SB} , the number of SNe per SB, N_{SB} , and the energy efficiency of SBs, ϵ , which in turn may depend on each other and on other parameters in ways that are difficult to constrain with current knowledge. Thus, above, we neglected SN clustering, i.e. we adopted $f_{\text{SB}} = 0$. [Chamandy & Shukurov \(2020\)](#) find that this assumption does not drastically alter the values of the turbulence parameters, typically making τ about 2–3 times smaller and l about 2 times smaller compared to the fiducial case $f_{\text{SB}} = 3/4$, whereas u is similar in the two cases. Nevertheless, SBs may sometimes be important, so in Section A.2 we formulate the equations for $f_{\text{SB}} \neq 0$. The mean vertical outflow speed U_0 is likely affected by SBs, so may itself depend on f_{SB} , N_{SB} and ϵ .

A.1. Including mean vertical outflows

This section generalises the magnetic field model of Section 3 to include a galactic outflow, with outflow speed U_0 .

Using an expression from [Hollins et al. \(2017\)](#) we can write

$$\sigma_z \simeq \sigma_r \left[1 + \frac{K_U U_0 \tau}{l} \left(1 + \frac{1}{(1 + q\Omega\tau)^2} \right) \right]^{1/2}, \quad (\text{A1})$$

where U_0 is defined to be equal to the mean vertical outflow speed at the disk surface $z = \pm h$, with h the scale height of the gaseous disk, and K_U a constant of order unity. As it represents an average for the entire disk, the quantity U_0 should be taken as the mass-weighted, area-averaged outflow speed, and has been estimated to be in the range 0.2–2 km s⁻¹ for spiral galaxies ([Shukurov et al. 2006](#)).

Substituting equations (4) and (A1) into the expressions for b and b_{iso} , and setting $K_U = 1$, we obtain

$$b_{\text{ani}} \equiv \sqrt{b^2 - b_{\text{iso}}^2} = \frac{1}{\sqrt{3}} \left[2q\Omega\tau \left(1 + \frac{q\Omega\tau}{2} \right) + \frac{U_0\tau}{l} \left(1 + \frac{1}{(1 + q\Omega\tau)^2} \right) \right]^{1/2}. \quad (\text{A2})$$

The mean magnetic field strength in the saturated state is now given by

$$\bar{B} \equiv |\bar{\mathbf{B}}| = K B_{\text{eq}} \chi(p) \left(\frac{D}{D_c} - 1 \right)^{1/2} \frac{l}{h} \left(R_U + \pi^2 R_\kappa \right)^{1/2}. \quad (\text{A3})$$

where we make use of the Reynolds-type dimensionless number

$$R_U \equiv \frac{U_0 h}{\eta}. \quad (\text{A4})$$

The critical dynamo number is now given by

$$D_c = - \left(\frac{\pi}{2} \right)^5 \left(1 + \frac{1}{\pi^2} R_U \right)^2. \quad (\text{A5})$$

Additionally, we have

$$\chi(p) = \left(2 - \frac{3 \cos^2 p}{2\sqrt{2}} \right)^{-1/2}, \quad (\text{A6})$$

where

$$\tan p_B = \frac{\bar{B}_r}{\bar{B}_\phi} = \frac{\pi^2 + R_U}{4R_\Omega} = - \frac{\pi^2 \tau u^2 + 6h U_0}{12q\Omega h^2}, \quad (\text{A7})$$

and p_B is the pitch angle of $\bar{\mathbf{B}}$, defined such that $-\pi/2 < p_B \leq \pi/2$ with $p_B < 0$ for trailing spirals. Note that $\chi \approx 1$, depending only weakly on p_B . Given the uncertainties of the model, this dependence is inconsequential, and thus we set $\chi = 1$. The quantity K in equation (A3) is an adjustable parameter of the model.

A.2. Including superbubbles

This section summarizes the SN-driven turbulence model of [Chamandy & Shukurov \(2020\)](#). For an overall SN rate per unit volume ν , the rate per unit volume of isolated SNe is given by

$$\nu_{\text{SN}} = (1 - f_{\text{SB}}) \nu, \quad (\text{A8})$$

where f_{SB} is the fraction of SNe in SBs, and that of SBs is given by

$$\nu_{\text{SB}} = \frac{f_{\text{SB}} \nu}{N_{\text{SB}}}, \quad (\text{A9})$$

where N_{SB} is the mean number of SNe in a given SB. [Higdon & Lingenfelter \(2005\)](#) estimate that the fraction of SNe occurring in OB associations is $\sim 3/4$ for the Milky Way, which suggests $f_{\text{SB}} \sim 3/4$ for our Galaxy.

A.2.1. Turbulent correlation length l

The turbulent correlation length is estimated as

$$l = \left(\frac{\Gamma - 1}{\Gamma} \right) C_l l_{\text{SB}} \left(\frac{1 + (l_{\text{SN}}/l_{\text{SB}}) \dot{E}_{\text{SN}}^i / \dot{E}_{\text{SB}}^i}{1 + \dot{E}_{\text{SN}}^i / \dot{E}_{\text{SB}}^i} \right), \quad (\text{A10})$$

where l_{SN} and l_{SB} are the driving scales for isolated SNe and SBs, respectively, and \dot{E}_{SN}^i and \dot{E}_{SB}^i are their respective energy injection rates. For Kolmogorov turbulence, $\Gamma = 5/3$, and C_l is a constant of order unity that comes from turbulence theory – below we adopt $C_l = 3/4$ (Monin & Yaglom 2007).

For SBs, we identify the driving scale of turbulence with the final radius reached by an SB in the midplane of the galaxy,

$$l_{\text{SB}} \approx \min \left[R_{\text{SB}}(t_s^{\text{SB}}), \lambda h \right], \quad (\text{A11})$$

where the first case corresponds to deceleration to c_s and the second case to blowout from the disk. Here t_s^{SB} is the SB age for which the SB expansion has slowed to the ambient sound speed (if it has not blown out), λ is a parameter of order unity, and

$$R_{\text{SB}}(t_s^{\text{SB}}) = 0.53 \text{ kpc } \epsilon_{0.1}^{1/3} N_{100}^{1/3} E_{51}^{1/3} n_{0.1}^{-1/3} c_{10}^{-2/3}, \quad (\text{A12})$$

where $0.1 \epsilon_{0.1}$ is the fraction of the SB energy that is mechanical and $N_{100} = N_{\text{SB}}/100$.

The ratio of the rates of energy per unit volume injected by isolated SNe and SBs is $l_{\text{SN}}^3 \nu_{\text{SN}} / l_{\text{SB}}^3 \nu_{\text{SB}}$, which gives

$$\frac{\dot{E}_{\text{SN}}^i}{\dot{E}_{\text{SB}}^i} = \begin{cases} 0.63 \left(\frac{3(1-f_{\text{SB}})}{f_{\text{SB}}} \right) \epsilon_{0.1}^{-1} E_{51}^{-1/17} n_{0.1}^{-2/17} c_{10}, & \text{if } t_s^{\text{SB}} \leq t_b^{\text{SB}}; \\ 1.47 \left(\frac{3(1-f_{\text{SB}})}{f_{\text{SB}}} \right) N_{100} E_{51}^{16/17} n_{0.1}^{-19/17} c_{10}^{-1} \lambda^{-3} h_{0.4}^{-3}, & \text{if } t_b^{\text{SB}} < t_s^{\text{SB}}. \end{cases} \quad (\text{A13})$$

Here t_b^{SB} is the age of the SB when it blows out of the disk (if it in fact blows out). The similarity solution for SBs yields, from $\dot{R}_{\text{SB}}(t_s^{\text{SB}}) = c_s$,

$$t_s^{\text{SB}} = 31 \text{ Myr } \epsilon_{0.1}^{1/3} N_{100}^{1/3} E_{51}^{1/3} n_{0.1}^{-1/3} c_{10}^{-5/3}. \quad (\text{A14})$$

From $R_{\text{SB}}(t_b^{\text{SB}}) = \lambda h$, we find

$$t_b^{\text{SB}} = 15 \text{ Myr } \epsilon_{0.1}^{-1/2} N_{100}^{-1/2} E_{51}^{-1/2} n_{0.1}^{1/2} \lambda^{5/2} h_{0.4}^{5/2}, \quad (\text{A15})$$

where $h_{0.4} = h/(0.4 \text{ kpc})$.

A.2.2. Root-mean square turbulent velocity u

Applying the method briefly outlined in Section 4.2 to the case $f_{\text{SB}} \neq 0$, we obtain the general expression

$$u = \left[\frac{4\pi}{3} l c_s^2 \nu \left((1 - f_{\text{SB}}) l_{\text{SN}}^3 + \frac{f_{\text{SB}}}{N_{\text{SB}}} l_{\text{SB}}^3 \right) \right]^{1/3}. \quad (\text{A16})$$

A.2.3. Turbulent correlation time τ

The quantity τ_r is the time for the flow to renovate due to the passage of an SN or SB blast wave. The renovation rate is equal to the sum of the rates from isolated SNe and SBs, so the renovation time is given by

$$\tau_r = \left(\frac{1}{\tau_{\text{SN}}^r} + \frac{1}{\tau_{\text{SB}}^r} \right)^{-1}. \quad (\text{A17})$$

A generalisation of equation (28) to $f_{\text{SB}} \neq 0$ gives

$$\tau_{\text{SN}}^r = 6.8 \text{ Myr } \left(\frac{1}{4(1 - f_{\text{SB}})} \right) \nu_{50}^{-1} E_{51}^{-16/17} n_{0.1}^{19/17} c_{10}, \quad (\text{A18})$$

where $\nu_{50} = \nu/(50 \text{ kpc}^{-3} \text{ Myr}^{-1})$. The renovation time for SBs is equal to $3/(4\pi l_{\text{SB}}^3 \nu_{\text{SB}})$, which gives

$$\tau_{\text{SB}}^r = \begin{cases} 4.3 \text{ Myr } \left(\frac{f_{\text{SB}}}{3/4} \right)^{-1} \nu_{50}^{-1} \epsilon_{0.1}^{-1} E_{51}^{-1} n_{0.1} c_{10}^2, & \text{if } t_s^{\text{SB}} \leq t_b^{\text{SB}}; \\ 9.9 \text{ Myr } \left(\frac{f_{\text{SB}}}{3/4} \right)^{-1} \nu_{50}^{-1} N_{100} \lambda^{-3} h_{0.4}^{-3}, & \text{if } t_s^{\text{SB}} > t_b^{\text{SB}}. \end{cases} \quad (\text{A19})$$